Physical Modelling of Gas Stirred Metallurgical Reactors Containing Two Liquids

Dominic Verhelst

Department of Mining and Metallurgical Engineering
McGill University
Montreal, Canada
January 1991

A Thesis Submitted to the
Faculty of Graduate Studies and Research
in Partial Fulfillment of the Requirements for the
Degree of Master of Engineering

ABSTRACT

Small, intensive metallurgical reactors are becoming more desirable because of their high relative production rates and rapid process kinetics. At pyrometallurgical operating temperatures, chemical reactions are virtually instantaneous. Therefore intensive processes require intensive mixing of the molten material, and intimate contact between reacting phases, to maximize mass and heat transport phenomena. The present work represents a study of the mixing and slag entrainment behaviour of lightly, and intensively stirred, metallurgical processes through the use of physical modelling. Two immiscible fluids were mixed in a model reactor having an aspect ratio of 0.33, and equipped with a single centrally located tuyere, through which air was blown. The thickness of the upper, less dense liquid layer varied up to 1/4 of the depth of the bulk liquid. Scaling of air flowrates between the model and prototype reactors was achieved using a modified Froude number modelling criterion Dye injection was used to monitor and characterize the mixing behaviour, while the entrainment of the upper phase was measured by continuously extracting liquid from the model and passing the fluid through an optical sensor system designed and constructed for the study

For low energy input systems, it was found that the thickness of the second liquid phase can significantly affect the mixing time of the bulk phase by altering the fluid flow pattern of the liquid. At higher gas flowrates, the thickness of the upper phase does not greatly affect this behaviour. The entrainment of the upper phase into the lower phase was also affected by the thickness of the upper phase, as well as by the intensity of bath agitation. At low flowrates, the number density of entrained droplets was constant with time, increasing with increasing agitation and thickness of the layer. For the intensively stirred cases, the number density of entrained droplets increased with time until a very high density of small droplets was reached, at which time the number of droplets once again became constant. The air flow required for the transition in the entrainment behaviour increased with an increase in the thickness of the upper phase.

RÉSUMÉ

Les petits réacteurs métallurgiques de haute intensités ont récemment évoqué beaucoup d'intérêt dû à leur taux de productivité relativement élevé et à leurs cinétiques rapides. Les réactions chimiques, aux températures des opérations pyrométallurgiques, sont quasiment instantanées. Alors, ces processus intenses nécessitent le malaxage intense des matières en fusion. Un intime contact entre les phases réagissantes est requis pour maximiser les phénomènes du transport de masse et de chaleur. Ce travail réprésente une étude des caractéristiques du malaxage et de l'entraînement du scorie dans un procédé métallurgique, d'après un modèle physique. Deux liquides immiscibles étaient mélangées dans un modèle de réacteur ayant un rapport d'allongement de 0.33, et pourvu d'une tuyère fixé au centre du modèle. L'épaisseur de la couche de liquide supérieure (moins dense) varie jusqu'à 1/4 du hauteur de la liquide inférieure (plus dense). Le facteur d'échelle, pour calculer le débit d'air du modèle correspondant à celui du prototype, était déterminé utilisant comme critère un numéro de Froude modifié. L'injection de la tenture était utilisée pour surveiller et caractériser le malaxage. L'entraînement de la phase supérieure était mesuré par l'extraction continue de liquide. Cette liquide était envoyée à un senseur optique concu pour cette étude.

Pour les systèmes avec une faible puissance d'entrée, l'épaisseur de la couche de la phase liquide supérieure influence d'une façon significative l'écoulement et le refoulement de la liquide, et ainsi le temps de malaxage. Par contre, à des débits d'air élevés, l'influence de l'épaisseur de la couche est minime. L'entraînement de la phase supérieure dans la phase inférieure est influencé par l'épaisseur de la couche supérieure et par l'intensité d'agitation du bain. A des débits d'air faibles, la densité de nombre des gouttelettes entraînées était constante avec le temps mais augmentait avec l'agitation croissante et avec l'épaisseur de la couche supérieure croissante. Pour les systèmes très bien agités, la densité de nombre augmentait avec le temps jusqu'au point où une très haute densité de petites gouttelettes est atteinte. A ce moment-ci le nombre de gouttelettes devient constant. Le débit d'air requis pour la transition du tenue de l'entraînement augmente avec l'accroissement de l'épaisseur de la couche de la phase supérieure.

ACKNOWLEDGEMENTS

I would like to take this opportunity to express my appreciation to some of the people who have contributed in various ways throughout the duration of my time at McGill University.

My sincere thanks are given to Dr. Rod Guthrie for accepting me as a member of his research team and for offering his guidance, knowledge and friendship. In particular, I wish to acknowledge his patience during the time that this document was prepared.

Frank Sebo, the resident magician and technician in the group, was responsible for many of the gadgets used in this study. His efforts, friendship (and daily pot of tea) were invaluable to me I will always treasure my time at McGill because of him.

I wish to thank Carol Jefferies for transforming my attempt at a french abstract into an understandable group of words.

Joe McDermid and Bahadır Kulunk are two friends who offered timely help, and endless entertainment (and the occasional brew). I thank you both.

Finally, I wish to thank my parents for their continual support and understanding during my academic life. They may not have always understood me when I tried to explain the world of metallurgy, but they were always close at hand when I needed help.

Dominic Verhelst

TABLE OF CONTENTS

LIST OF FIGURES

LIST OF TABLES

NOMENCLATURE

A	area
d	tuyere diameter
g	gravitational constant
h, H	bath depth
k	constant of proportionality
L	characteristic length, reactor height
M	mass flowrate
n	flowrate exponent in mixing time equation
P	pressure
Q	flow rate
r	plume radius
R	reactor radius
T	temperature
u, U	velocity
$\bar{u}$	mean velocity
V	volume
α	gas fraction in two phase plume
ε	energy dissipation (W/m^3)
λ	linear dimensional scaling factor ($L_{model}/L_{full\ scale}$)
υ	viscosity
ρ	density
σ	surface tension
τ	mixing time

Subscripts

g	gas
l	liquid
l1	higher density liquid
l2	lower density liquid
p	plume

1 INTRODUCTION

1 1 Evolution of Gas Injection Metallurgy

Throughout the development of pyrometallurgical processes, the forced injection of gas into furnaces has been the keystone to many advances. This is clearly demonstrated in the evolution of steelmaking when, in the 1800's, both Bessemer and Thomas discovered that air injected into a bath of molten pig iron produced a steel of higher quality much faster than the conventional technique using puddle furnaces At the time it was unclear as to why forced air injection had a heating, rather than a cooling, effect on the melt and why the product was of greater and more consistent quality [1] However, as the levels of knowledge and technology increased, it became understood that injected gases could be used for two purposes. (a) as a reactant and a powerful source of heat, and (b) as a stirring agent producing increased process kinetics and improved homogeneity. This understanding then led to rapid progress in the production and refining of not only steel but also of non-ferrous metals produced pyrometallurgically

In the area of iron and steelmaking, process improvements, through the control of bath stirring, have been applied to almost every reaction vessel Kato[2] has reviewed the changes in the primary steelmaking process from the Open Hearth furnace to the top blown converters and subsequently to the Q – BOP and combination blown converters The author concluded that improved mixing is responsible for these advances and that submerged injection produces the most efficient stirring Submerged gas injection through tuyeres and various designs of porous plugs has also redefined the purpose of the ladle and led to the growth of secondary refining in the steelmaking sequence The ladle has evolved from being just a transfer to being a reaction vessel for the removal of inclusions, the addition of alloying and deoxidation elements and, with the use of vacuum systems, the removal of deleterious dissolved elements.[3] Processes for the bath smelting of iron ore fines using submerged gas injection are currently being developed [4] Such smelting processes allow for smaller scales of production, as compared to the conventional large blast furnaces, and could aid in the growth of smaller

ironmaking facilities to decentralize the production and distribution of virgin steel.

For the production of non-ferrous metals, submerged gas injection is being used in new smelting and converting processes. During the past two decades, bath smelting techniques have arisen to replace conventional blast and reverberatory furnaces for the smelting of copper[5]. These bath smelters include the Noranda and Mitsubishi processes which use submerged gas injection in to continuous reactors. More recently, the QS and QSL reactors have come onto the scene as channel reactors, incorporating submerged gas injection, for the continuous production of copper and lead, respectively. Not all new non-ferrous processes are continuous. Both the Sirosmelt and Kaldo operations are batch processes. In the Sirosmelt reactor, used for the two stage production of copper, lead and tin, air or oxygen is injected via a partially submerged lance into a molten bath held in a stationary vertical cylindrical vessel.[6] The Kaldo operation uses a top blown rotary converter (TBRC) to intially flash smelt the concentrate, followed by further bath smelting. As with developments in the steel industry, these new processes aim to improve productivity through the use of forced gas injection.

In 1975, Richardson[7] compared old and new metallurgical processes on the basis of their volumetric intensity, defined as the mass of product extracted from a reactor per unit time per unit volume of the reactor . Table 1.1 summarizes some of the results. A comparison of the values of the volumetric intensities for the reverberatory furnace and the Noranda process, as well as for the open hearth furnace and the Q-BOP converter, shows that increased bath agitation greatly increases product throughput. These improvements are a result of enhanced stirring (for effective thermal and chemical homogenization) and of increased interaction between the various phases in the vessel (which improves process kinetics). A study by Berg et al.[8] on desulphurization in steelmaking ladles also concluded that process efficiency can be significantly affected through stirring and increased contact between the metal and slag phases.

From the description of recently developed and emerging processes, it would appear that submerged gas injection, via either tuyeres or a partially

Table 1.1 Volumetric Intensity for Various Pyrometallurgical Processes [7]

Process	Volumetric Intensity ($t/m^3/min$)
Reverberatory Furnace	0.0007
Open Hearth Steelmaking	0.002
Copper Converting	0.004
Noranda Process (Enriched Air)	0.005
Anode Refining of Copper	0.008
Harris Lead Refining	0.03
Basic Oxygen Furnace for Steel	0.05
Bottom-Blowing Oxygen Converter for Steel	0.07
Spray Steelmaking	0.10
Spray Degassing of Steel	0.15

submerged lance, has become the method of choice for stirring a molten bath or introducing reactants into a vessel. Therefore, in order to analyze new and existing processes on such a basis, it is important to gain some understanding of the fluid flows generated in the reaction vessel and the interactive behaviour of the different phases present.

1.2 The Dynamics of Gas Injection Processes

The subject of fluid dynamics is very important to process efficiency since the flow of molten material, largely as a result of inert gas stirring, will control the chemical and thermal homogenization of the molten material and the efficient use of alloy additions. Also, process kinetics are dependent on the efficient transport of reactants to, and products away from, reaction zones near gas plumes and at slag-metal, or slag-matte, interfaces. Many studies have shown that the dispersion of material is influenced by both macroscopic convective currents and localized turbulent diffusion.[9,10,11]

In an ongoing attempt to understand the many variables affecting the dynamics of gas stirred vessels, previous investigators have used physical and mathematical modelling techniques to study the structure of gas plumes, and its relation to fluid flow. The nature of the flow then influences the efficiency of overall bath mixing and the interactions between phases.

1.2.1 Analysis of the Gas Plume and Fluid Flow

When studying processes involving submerged gas injection it is essential to understand the nature of the buoyant plume and how it generates a recirculatory flow within the the vessel. Gas exiting a submerged lance, nozzle, or porous plug, breaks up into a stream of bubbles. As gas bubbles rise surrounding liquid is dragged upwards in their wake, producing a buoyant plume comprised of gas and liquid. As the plume rises, it expands to form a somewhat conical shape. Extensive measurements of the structure (i.e. gas fraction) of turbulent plumes were performed by Castillejos and Brimacombe.[12] They concluded that for virtually the entire plume a relatively simple equation describes the normalized gas voidage, α/α_{max}, at any given normalized radial position, $r/r_{\alpha_{max/2}}$, within the plume:

$$\frac{\alpha}{\alpha_{max}} = exp\left| -0.7\left(\frac{r}{r_{\alpha max/2}} \right) \right| \qquad (1.1)$$

The term α_{max} refers to the maximum gas fraction in any given horizontal cross-section of the plume, which occurs at the center of the plume.

The authors also presented more complicated expressions for α_{max} and $r_{\alpha_{max/2}}$ as functions of the modified Froude number and axial position along the plume length. An area-wise averaging of the normalized gas fraction shows that the average gas fraction in any given horizontal plane of the plume is approximately 16 percent of the maximum voidage in that plane Using an average maximum gas fraction in the axial direction, from the authors' empirical equations, it was found that the average gas voidage in the plume ranges from 2 to 6 percent of the total plume volume, depending upon the modified Froude number (i.e. gas flowrate) used. The results of this analysis agree well with the values of total gas fraction of 2 to 10 percent reported by Sahai and Guthrie[13] who estimated the gas voidage by dividing the volume of gas in the plume by the total plume dimensions The plume volume was calculated assuming that the plume was cylindrical, the diameter of which was the mean diameter of the more realistic conical plume The volume of gas in the plume was calculated according to the equation

$$V_g = Q_g * \frac{h}{u} \qquad (1.2)$$

The gas flow rate, Q_g, was corrected for temperature and pressure and the vertical plume velocity, $\bar{u}$, was related to the rise velocity of a bubble in liquid. Therefore, the entrainment of liquid by the rising plume is significant and is responsible for the generation of bulk convection within the bath.

According to the results of studies by Hussain and Siegel[14] of gas injection through a single centrally located tuyere in the bottom of an vertical cylindrical vessel, the entrainment of liquid into the two-phase plume by the rising gas bubbles accounts for less than 1 percent of the mass of the

pumped liquid and that liquid-liquid entrainment is the dominant mode of fluid pumping. At the point of gas injection, some liquid is put into motion in the wake of the rising bubbles. Subsequently, additional fluid is entrained, not by the gas bubbles but by the now moving liquid in the plume. According to Castillejos and Brimacombe liquid entrainment is greatly enhanced after the value of α_{max} falls below approximately 70 percent.

As the plume reaches the free surface of the bath, the liquid which was pumped upwards is diverted radially outwards towards the vessel wall, where it is again rediverted downwards along the wall. In this manner a recirculatory flow is generated, as depicted in Figure 1.1.

Hussain and Siegel also derived an empirical relation between the mass flowrate of liquid in the plume being pumped to the free surface and the mass flowrate of injected gas.

$$M_l \propto M_g^{0.4} L^{1.4} \tag{1.3a}$$

Introducing the densities of the liquid and gas phases, this equation becomes:

$$Q_l \propto Q_g^{0.4} L^{1.4} \left(\frac{\rho_g}{\rho_l} \right)^{0.4} \tag{1.3b}$$

The rate at which liquid is pumped by the plume is directly related to the speed of recirculation of the bulk fluid, which in turn is related to the time required for chemical or thermal inhomogeneities within the fluid to be reduced. An average recirculation time of the bath fluid can be defined as the total volume of the bath divided by the volume flow rate of liquid pumped by the plume. Sano and Mori[15] have stated that in order for a sudden addition of a tracer material to be completely, and evenly, distributed throughout the bath, an average of three circulations of the bath liquid is required. This time for homogenization was defined as the mixing time. From the findings of Hussein and Siegel, together with the definition of the

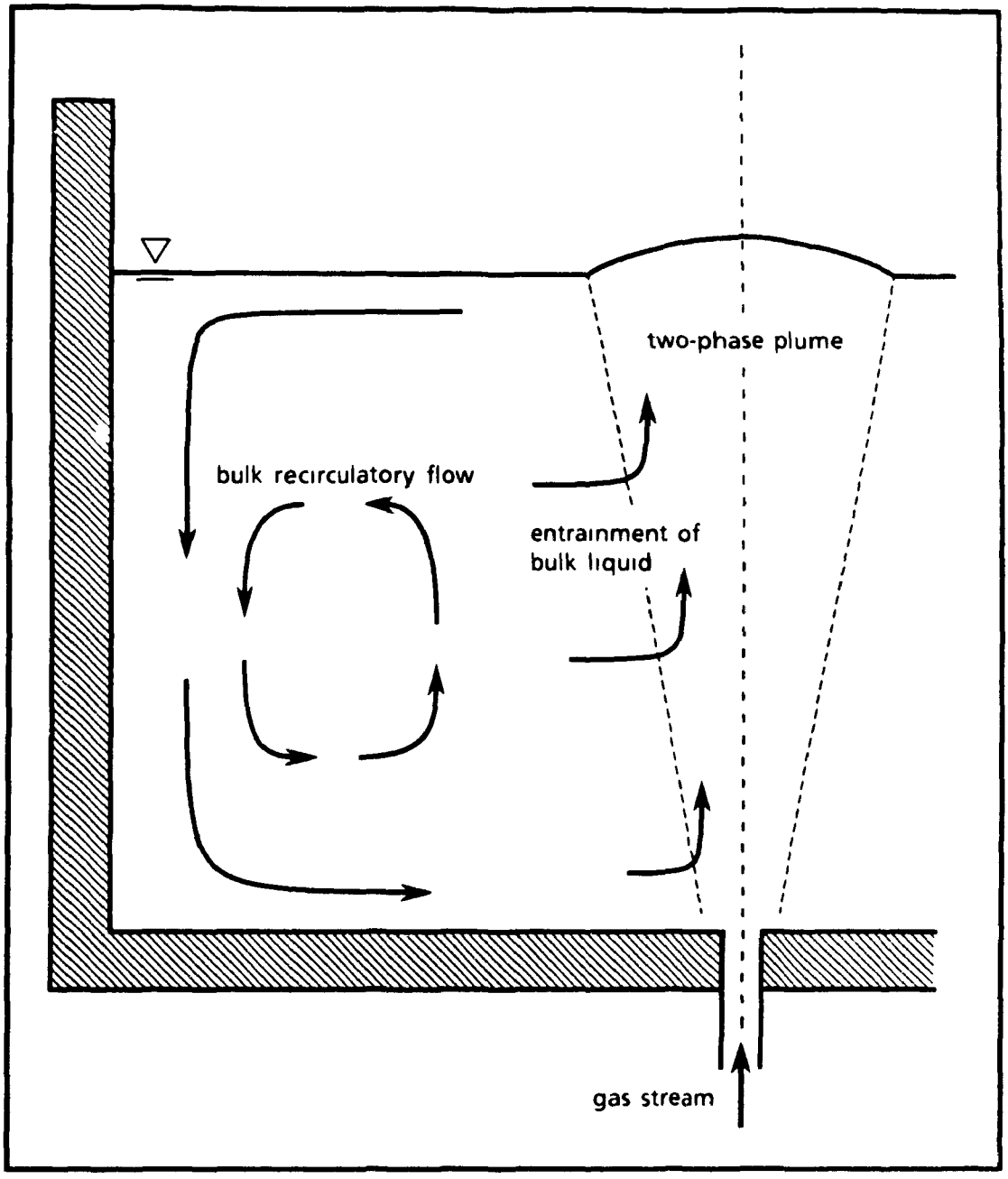

Figure 1.1. Representation of Plume Formation and Fluid Recirculation in Gas Stirred Systems

recirculation time, it can be shown that this mixing time is related to the volumetric flowrate of injected gas according to the equation:

$$\tau_{mix} = 3\tau_{recirc} = 3\frac{V_{bath}}{Q_l} = kQ_g^{0.4} \qquad (1.4)$$

where k is a constant of proportionality. This equation offers some insight into the mixing process in an upright cylindrical tank as derived from an analysis of the structure of the centrally located rising two-phase plume.

1.2.2 Mixing Behaviour

Since bath mixing is an important feature in process operations and globally characterizes the fluid motion in a vessel, many investigations have been carried out to determine the relationship between gas flowrate and mixing time in various metallurgical vessels using physical modelling techniques. Rather than measuring the pumping rate of the plume, bath homogenization is monitored directly by measuring "the time required to reduce a suddenly created concentration difference between two points to an insignificant value".[16]

Various techniques for measuring the mixing time have been developed, and are discussed in more detail in the next chapter. These studies have concluded that for upright cylindrical vessels with a single centrally located tuyere or submerged lance the mixing time is related to the volumetric gas flowrate according to the relationship:

$$\tau_{mix} = kQ^{-n} \qquad (1.5)$$

where k and n are positive, non-zero constants. Many values for the gas flowrate exponent, n, have been quoted, ranging from 0.19 to 0.49 A summary of experimentally determined values of n is given in Table 1.2, along with values of n derived from mathematical models. As can be seen from these results, the average value of the flowrate exponent agrees well

Table 1.2 Values for the gas flowrate exponent, n, with respect to the mixing time, τ, for various systems

Technique	Flowrate Exponent (n)	Reference
Mathematical Modelling	– 0.33	10
	– 0.337	15
Pilot or Full Scale Tests	– 0.25	17
	– 0.40	18
	– 0.40	19
Physical Modelling* (Single Fluid)	– 0.2	20
	– 0.23 (H/D = 0.25) – 0.19 (H/D = 1.0)	21
	– 0.32	22
	– 0.32	23
	– 0.34	10
	– 0.39	24
	– 0.46	25
	– 0.49 (H/D = 0.5)	26
Physical Modelling* (Slag Layer Simulated)	– 0.262 (no slag) – 0.243 (with slag)	27
	– 0.31 (no slag) – 0.42 (with slag)	19
	– 0.32 (no slag) – 0.43 (with slag)	28

* Unless otherwise indicated, the aspect ration (H/D) used in the study was approximately 1.0

with the empirical value of 0.4 determined by Hussain and Siegel based upon their analysis of the pumping capacity of a two-phase plume.

However, a fundamental difference exists between the analysis of Hussain and Siegel and the direct measurement technique used by others. As was mentioned, mixing and dispersion in a stirred melt is controlled by convective flow and turbulent diffusion. After extensively studying mixing in gas stirred steelmaking ladles, Mazumdar and Guthrie[10] concluded that mixing cannot be characterized entirely by either of these two modes. The definition of the mixing time as described by equation 1.4 was based upon the measurement of liquid flow in a plume and the concept of overall bath turn-over and does not consider turbulence within the bath nor the shape of the vessel. It would appear, therefore, that equation 1.4 describes the mixing behaviour exclusively in terms of bulk convection. In contrast, in the direct measurement process, mixing is monitored at one or more points in the bath Therefore, the combined influence of convection and diffusion is measured and the two modes cannot be easily separated quantitatively

Many pyrometallurgical operations involve the injection of gas into a reactor containing two immiscible liquids. However, despite the extensive investigations of mixing in submerged gas injection processes which have been undertaken in the past, most of which seem to concentrate on ladle operations, very little information is available on the influence of a less dense second liquid phase, such as a slag layer in ladles, on mixing behaviours. Mazumdar, Nakajima and Guthrie[29] have shown, that the presence of an upper layer of liquid results in a slight alteration in fluid flow patterns and a reduction in the fraction of the input energy used to generate fluid flow. According to the authors, some of the energy input to the system by the injected gas is dissipated by the creation and entrainment of droplets of the upper phase and a distortion of the liquid-liquid (slag/metal) interface, with the latter dissipating by far the greatest fraction of energy The loss of energy causes a general increase in the mixing time[19,28], but does not appear to greatly affect the flowrate exponent in equation 1.3, as is indicated by the results quoted in Table 1.2. The values quoted, however, were determined over the narrow range of energy inputs associated with ladle metallurgy operations and may not be applicable to intensively stirred reactors, such as

converters. Under intensive stirring conditions, the level of turbulence is much higher and mixing should be greatly enhanced, regardless of the presence of the second phase. Unfortunately, data on mixing in such reactors are scarce.

1.2.3 Mass Transfer and Interactions Between Phases

Gas injection is not only used for chemical and thermal homogenization, but also to transport reactants to, and products from, reaction interfaces, such as slag-metal, matte-slag and bubble-liquid contact areas. Using different chemical systems, various investigators have modelled the mass transfer of various tracer chemicals across interfaces between immiscible fluids.[28,30-32] The results of liquid-liquid mass transfer studies indicate that the interphase mass transport coefficient is correlated to the volumetric gas flowrate according to the power law:

$$kA \propto Q^n \qquad (1.6)$$

where the product, kA, is termed the "capacity coefficient" or the "mass transport conductance" and n is a positive constant. Mataway et al.[30] reported a value of 1.0 for n, while Kim and Fruehan[28] concluded that the value of n changes dramatically from 0.6 to 2.51, and again to 1.43. The shifts in the value of n occur at specific critical gas flowrates and are believed to be due to the generation and entrainment of droplets of the upper phase into the more dense phase, thereby increasing the area available for mass transfer.

Berg et al.[8] measured the desulphurization of steel in a ladle under the influence of both gas and inductive stirring. They also noticed a sudden increase in the value of n at a specific gas flow, but no comparable shift when inductive stirring was used. The change in behaviour was concluded to be a result of slag entrainment into the steel when gas stirring was employed, which is not likely to occur when the bath is inductively stirred. Kim and Fruehan attempted to calculate the interfacial surface area from measurements of the capacity, kA, and average values of the mass transport coefficient, k, determined for their specific chemical system. They then

compared these values to the planar interfacial area between the immiscible phases. A reproduction of their results (Figure 1.2) shows that as the flowrate increases, the estimated total interfacial area increases and greatly exceeds the calculated planar area. The reduction in area with increasing gas flowrate is a result of an increasing plume diameter. As the plume diameter increased, the amount of the upper phase cleared from the eye of the plume at the bath surface increases, thereby reducing the planar interfacial area. The material cleared away may either be entrained in the bath or simply displaced to produce a slightly thicker upper layer No attempt was made by the authors, however, to measure the size or distribution of entrained droplets to verify their estimated values.

A modelling study of combination blown steelmaking converters by Tanaka[33] has shown that slag droplet entrainment into molten steel is a result of the submerged gas injection and that gas impingement from above the melt does not generate such droplets. Figure 1.3 depicts one possible mechanism for droplet formation and entrainment. As the fluid in the two-phase plume is redirected at the slag/metal interface, the shearing action between the two liquids, coupled with the oscillation of the interface, produces slag ligaments which are subsequently separated from the slag layer. Bulk fluid motion then disperses these droplets throughout the bath

Tanaka devised an Electric Sensing Zone system for detecting the presence of, and estimating the size of, entrained oil droplets in his modelling experiments. From measurements of droplet size distributions, the author showed that the area of the dispersed upper phase particles does increase with an increase in bottom gas flowrate and, for the range of flowrates used, is proportional to the flowrate to the power 0.66. Unlike Kim and Fruehan, Tanaka did not report the occurrence of a critical gas flowrate for particle formation and entrainment, possibly since such rates were not within the range of flows used in the study.

1.3 Purpose of the Present Study

With the increased use of submerged gas injection in pyrometallurgical operations, it is important to understand the influence of rising gas plumes

on process efficiency. As was indicated previously, most prior physical modelling studies of such systems have only considered the bulk liquid phase and have ignored the influence of a second, less dense liquid phase on process efficiency However, virtually all operations do contain two liquids, either metal and slag, or matte and slag phases. Therefore, in the present study, the influence of a second liquid on the dynamics of gas stirred processes will be analyzed through the use of a room temperature physical model.

The first part of the present study will concentrate on the fluid flow patterns and mixing behaviour in the bulk liquid while subjected to submerged gas injection. The modelling study covers a wide range of stirring intensities, from gently stirred vessels, such as ladles, to strongly agitated converters The range of gas flowrates is also extended to incorporate intensively stirred reactors, such as some of the emerging non-ferrous processes in which emulsions and foams are prominent.

Following this, an analysis of the entrainment behaviour of the upper phase into the bulk liquid is made, as this phenomenom has been shown to greatly affect process kinetics. It is hoped that this information will help to fill in some of the gaps in the scarce data involving multiphase operations and aid in the understanding of current process dynamics, as well as give some insight into the efficiency of emerging pyrometallurgical processes

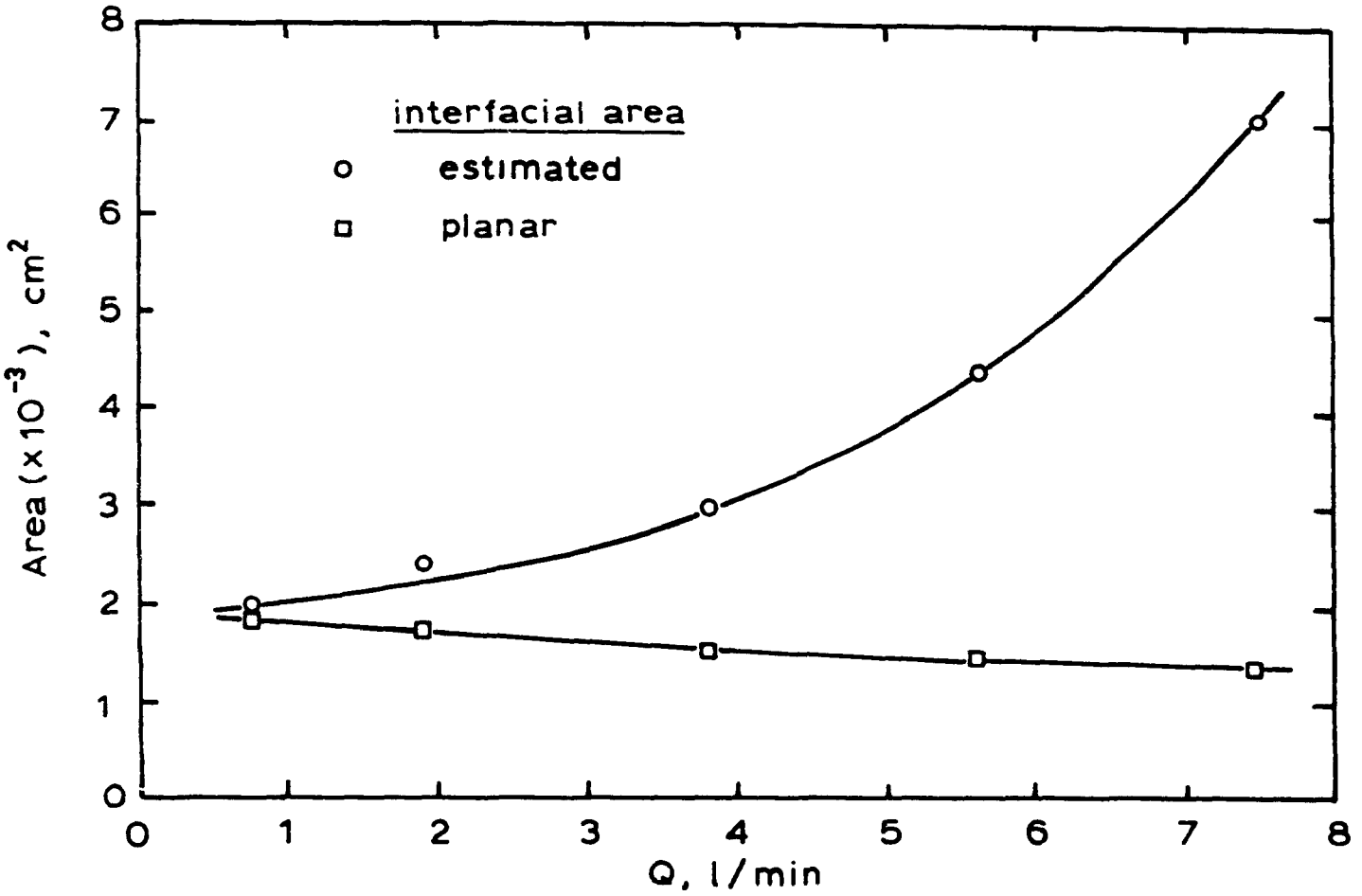

Figure 1.2 Liquid/liquid Interfacial Area vs Gas Flowrate for Gas Stirred Systems [28]

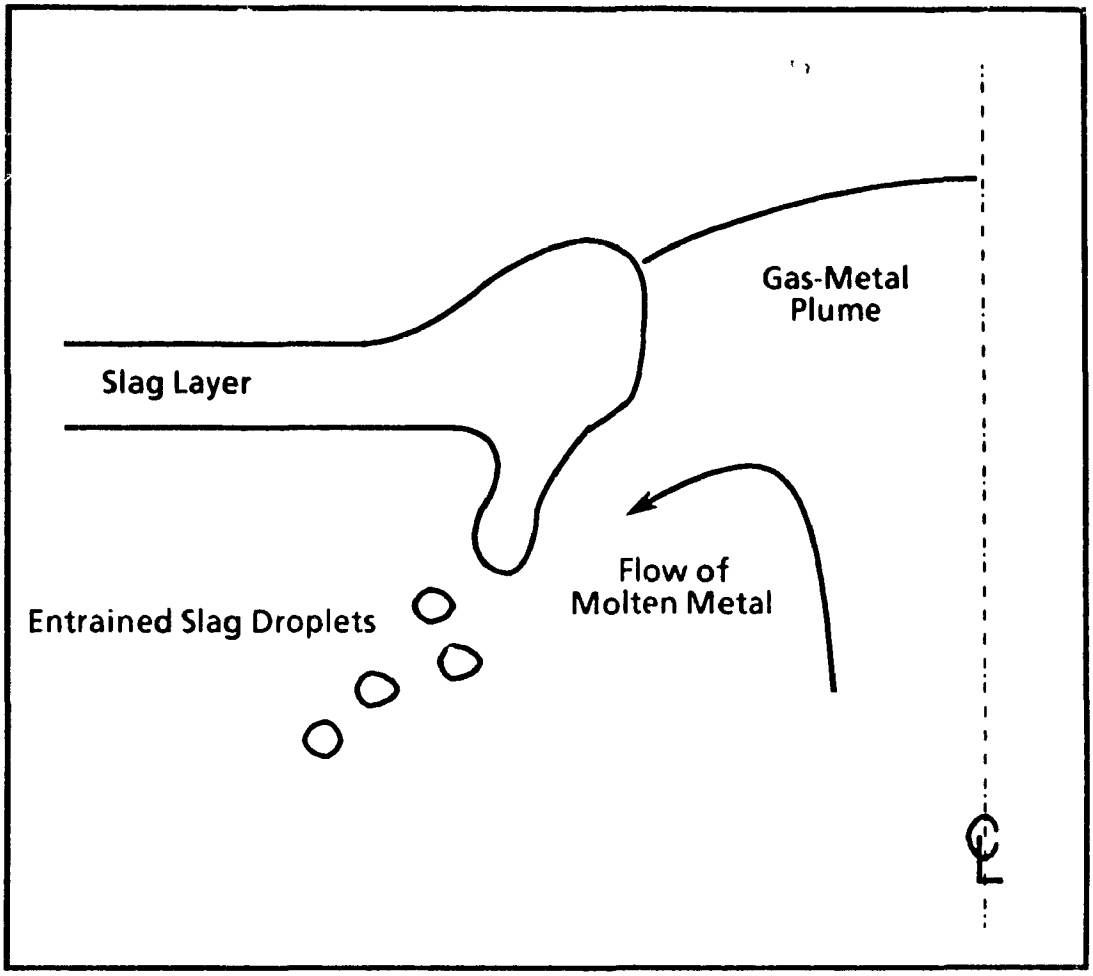

Figure 1.3. Possible Mechanism for the Formation and Entrainment of Slag Droplets in Molten Metal

2 EXPERIMENTAL PROCEDURES AND EQUIPMENT

The present study involved the physical modelling of gas stirred metallurgical reactors containing two immiscible liquids. The variables considered were: a) the mixing behaviour, i.e. mixing time as a function of gas flowrate, and b) the entrainment behaviour of the upper liquid into the lower liquid. The entrainment behaviour was described in terms of the number and sizes of entrained droplets, over a range of gas flowrates.

In the pyrometallurgical industry there are many different shapes and sizes of reactors and these are stirred by various means. However, as mentioned in the previous Chapter, submerged gas injection through tuyeres or porous plugs is becoming a very common method of bath agitation. Also, many of the reactor designs can be described as upright cylinders. This study will not be directed towards the modelling of any particular process, but, for simplicity, will concentrate on modelling a range of upright gas stirred cylindrical vessels. The range of gas flowrates used was chosen so as to encompass equipment such as a gently stirred ladles and highly agitated converters.

2.1 Principles of Physical Modelling

Physical modelling involves the use of one system of materials and equipment, with experiments typically performed at room temperature, in order to depict the events occurring in another system in which experiments are difficult to perform. Some reasons for these difficulties include high operating temperatures, opacity of liquids restricting the visualization of fluid flow, and possibly the presence of highly corrosive or toxic substances. Therefore, by substituting a room temperature model system for the real system, the measurement of desired parameters can become more manageable.

However, in order for the model to accurately describe the events occurring in the real system, it is important that certain conditions be satisfied. The two systems must be geometrically, mechanically and chemically similar. For geometric similarity, all dimensions of the model, such

as vessel diameter and bath depth, must be related to the real system according to the same linear scaling factor, λ, which is defined as the ratio of corresponding lengths between the model and the full scale system

Mechanical similarity may be divided into three catagories: static, kinematic and dynamic similarities. For the system under investigation in this study, static similarity, which is important when modelling the behaviour of structures, is not considered to be significant. The condition of kinematic similarity is satisfied when the paths traced out by corresponding particles in the two systems are geometrically similar for a corresponding time interval.[34] This offers a means of scaling time and was used by Kulunk[35] to scale the feeding rate of aluminum wire in a study of aluminum dispersion in gas stirred steelmaking ladles.

The third form of mechanical similarity, which is the most important in the present study, is dynamic similarity. In gas stirred systems, fluid motion is created as a result of rising gas bubbles, the speed of which is determined through the interaction of buoyancy, inertial and viscous forces. In addition, for systems containing two immiscible liquids, the interaction between the liquids is affected by the interfacial surface tension In order for the criterion of dynamic similarity to be assured, it is necessary for the ratio of corresponding dominant forces to be equal between the full scale and model systems.

Chemical similarity implies that the concentration of all chemical species in the model must bear a fixed relation to the full scale operation. This is important when modelling the distribution and reaction of constituents already present in a melt and any alloy additions made to the melt while the bath is being stirred. Chemical concentrations are controlled by initial concentrations, reaction rates, bulk fluid motion and molecular diffusion. As mentioned previously, bath homogenization, as measured by mixing behaviour, is regulated by bulk motion and eddy diffusion, and as such should be modelled according to a chemical similarity criterion. This criterion also requires that kinematic similarity be satisfied.

2.2 Modelling Criteria

In order to determine the operating parameters of a model, one must determine rules on which to base the parameters. One popular method is to specify important dimensionless quantities, containing the physical properties of the model and full scale systems, which describe the model in terms of the geometric and mechanical similarities listed above. Thus, in terms of the present system, the velocity of a liquid in buoyancy driven fluid flow is governed by the densities of the gas and bulk liquid, the viscosity of the bulk liquid, the depth of the bath and the acceleration due to gravity. The interfacial surface tension between two liquids, as well as the densities of the liquids, affect the nature of liquid/liquid interactions Using these important quantities and such techniques as the Buchingham π Theorem, it can be shown that the predominant forces involved in the system under study can be described by the following dimensionless ratios:

$$\text{modified Froude number} = \frac{\text{inertial force}}{\text{buoyancy force}} = \frac{\rho_g}{(\rho_l - \rho_g)} \frac{U^2}{gL} \tag{2.1}$$

$$\text{Reynolds number} = \frac{\text{inertial force}}{\text{viscous force}} = \frac{\rho UL}{\mu_l} \tag{2.2}$$

$$\text{Weber number} = \frac{\text{inertial force}}{\text{surface tension force}} = \frac{\rho U^2 L}{\sigma} \tag{2.3}$$

The best possible physical model is one in which the values of all corresponding dimensionless quantities are equal for the model and the full scale systems. However, in virtually all cases, the scale of the model and the choice of the simulation materials dictate that not all equalities can be maintained. For example, consider the case of argon injection into a ladle containing only molten steel being simulated by a 1/4 scale model of air injection into water. The physical properties of all substances involved are listed in Table 2.1. In this example the Weber number is not considered to be of significance since only one fluid is under investigation. It is necessary, then, to determine the required scaled gas jet velocity to be used in the model based upon the two remaining criteria. For a typical 150 tonne ladle

stirred by an argon flow of $1.88 \times 10^{-2} m^3/sec$ issuing from a 20.28mm diameter nozzle[36], the modified Froude and Reynolds numbers for the full scale ladle are 0 023 and 35386, respectively To calculate these values, the velocity , U, was defined as the average gas velocity at the tip of the nozzle and the characteristic length, L, was taken to be the bath depth For the calculated Froude number, an air flow of $2\ 41 \times 10^{-4} m^3/sec$ would be necessary in the model However, the Reynolds number for the model at this flowrate would be 10895 Similarly, modelling based on an equivalent Reynolds number would result in a Froude number of 0.243 for the model Therefore, for the simple model system chosen, it is impossible to satisfy both criteria

Table 2.1 Material Properties for Real and Model Systems

	Steel	Argon	Water	Air
Density (kg/m^3)	7000	1.65	1000	1 20
Viscosity ($kg/m\ s$)	$6\ 4 \times 10^{-3}$	-	$1\ 0 \times 10^{-3}$	-

Hence, it is important to determine on which basis the operating parameters of the model should be ascertained. This is accomplished by defining the dominant forces acting in the system. A comparison of the Reynolds and modified Froude numbers calculated for the 150 tonne ladle, which are the ratios of inertial to viscous and buoyancy forces, respectively, indicates that the buoyancy force greatly exceeds the viscous force. On this basis, it would seem appropriate that for gas stirred baths the modified Froude number should be used as the modelling criterion, from which the gas flowrate for the model can be calculated.

As stated above, the gas velocity at the tip of the tuyere as the air enters the bath was chosen as the characteristic velocity to be used in the calculation of the dimensionless quantities. For bouyancy driven flows this velocity will not always be a representative quantity since much of the kinetic energy of the gas is lost on entry into the bath. The result is Froude numbers which will

be slightly higher than which strictly represents the nature of the induced flow. The use of a superficial gas velocity, defined as the gas flowrate divided by the cross-sectional area of the bath generates Froude numbers which are exceptionally low. An alternative is to use the average plume velocity. This velocity more adequately describes the nature of the system. However, this velocity is difficult to determine. Therefore, for simplicity, and since no particular process is being modelled in this study, the tuyere gas velocity was chosen for all calculations. It is believed that the use of this velocity will provide a good range of model conditions.

2.2.1 Scaling of the Input Gas Flowrate

Since this study did not concentrate on the modelling of any particular process, but rather considered the influence of a second liquid layer on mixing and entrainment behaviour over a wide range of gas flowrates, it was necessary to determine upper and lower limits for the flowrate. The range of values should encompass the modelling of gas stirred ladles and converters. The Froude modelling criterion was used to determine the range of air flowrates necessary to model submerged gas injection into various steelmaking vessels. The modified Froude number for a 240 tonne Q-BOP, with 0.70m^3/sec of air injected through each of six 36mm diameter nozzles, is 6.36. This value, together with the value of 0.023 for an argon stirred ladle, was used to set the range of gas flowrates used in the experiments.

One model was built to study these greatly varying processes. All the vessels considered could be simulated by an upright cylindrical model having a flat base. Therefore, the linear scale factor, λ, for the various systems were not equal (i.e. λ = 1/20 for a Q-BOP and 1/10 for a ladle). The aspect ratio of the model (0.33), defined as the ratio of the bath depth to the vessel diameter, was chosen to have an intermediate value between that of ladle (0.7) and converter (0.23) operations. This was considered to be adequate since this study was concerned with the behaviour of liquid/liquid interactions in a general manner.

The model used for this study was constructed of a 300mm diameter upright plexiglass cylinder, with a height of 300mm. A square plexiglass box

was also built around the cylinder. Water was used to model the bulk fluid since its kinematic viscosity is very close to that of molten steel The water bath was 100mm deep and was stirred by air injected through a single 1 5mm diameter nozzle centrally located in the flat bottom plate of the vessel. For the modelling system chosen, a modified Froude number of 0 023 can be translated into an air flowrate of 7 66x10 - 6m3/sec (0.46l/min). Similarly, a value of 6.36 corresponds to 1.27x10 - 4m3/sec (7.6l/min) of air A range of 7.66x10 - 6 to 4.17x10 - 4m3/sec was selected for the study of mixing and entrainment behaviour for gently and intensively stirred reactors containing two liquids. Table 2 2 lists the flowrates used, together with their corresponding modified Froude and Reynolds numbers, as calculated by equation 2.1 and 2.2.

Table 2.2 Range of Gas Flowrates Used in Experiments

Gas Flowrate (litre/min)	Modifed Froude Number	Reynolds Number
0 46	0.023	532
1 42	0.22	1607
2 36	0.61	2671
5.0	2.72	5659
10 0	10.9	11318
15.0	24.5	16976
20.0	43.5	22635
25.0	68.2	28294

2.2.2 Selection of a Slag Simulation Fluid

The mechanical interaction between two agitated immiscible fluids, and the associated entrainment of one fluid into the other, is controlled largely by the densities of the two liquids, the interfacial surface tension between the liquids and the fluid velocity at the interface. This is described numerically by the Weber number, as stated by equation 2.3. The Bond

number, which is the ratio of buoyancy and interfacial surface tension forces could also be used as a possible criterion. The Bond number is described by equation 2.4. This criterion does not contain a velocity term, and therefore may be easier to apply since the velocity to be used is difficult to identify. Most oils have a density of 900-980 kg/m^3, as compared to 1000kg/m^3 for water. The respective values for slag and steel are 3000 and 7000 kg/m^3. With slag and steel having a typical equilibrium surface tension of 1.10N/m,[37] the modelling system would have to have an interfacial tension of appoximately 1.0×10^{-5}N/m to have an equivalent Bond number as the full scale system. This value is much lower than typical values for most oils and water, which are in the vicinity of 3×10^{-2}N/m.[38]

$$Bond\ Number = \frac{buoyancy\ force}{surface\ tension} = \frac{(\rho_{l1} - \rho_{l2})\, d^2 g}{\sigma} \qquad (2.4)$$

Gaye et al.[39] have reported that the surface tension between slag and steel can decrease as low as 0.3N/m for oxygen saturated steels during gas injection. The low value, which can even reach values close to zero, is thought to be a result of high mass transfer rates between the two phases. Therefore, the low value calculated for the model would have to be even lower. The use of a higher density bulk liquid, such as mercury or carbon tetrabromoethane, would produce higher values of interfacial tension in the model, but this option was rejected since the volume of liquid required for all experiments would have been too great.

The selection of a second liquid phase was based upon a similarity of physical properties, namely the kinematic viscosity, of slag and oil. Common SiO_2-CaO-FeO-Fe_2O_3 slags have viscosities of 2×10^{-5}m^2/s, however the viscosity can range from 2×10^{-5} to 5×10^{-4} m^2/s.[38] Chemical inertness with water was another factor considered in the selection since chemical reactions tend to change the interfacial properties of liquids. A dimethyl siloxane polymer, trade name Dow Corning® 200 Fluid, was selected. This oil is available in a wide range of viscosities (6.5×10^{-7} to 0.10m^2/s) with the specific gravity remaining constant at 0.96 throughout this range. The interfacial surface tension between water and this oil is also constant at

3.0×10^{-2}N/m. Two oils having dynamic viscosities of 2×10^{-5} and 5×10^{-5}m^2/s were used in the study

2.2.3 Experimental System

The physical model developed consisted of a 300mm diameter water bath, 100mm deep, covered with a layer of the silicon oil. The thickness of the upper phase was varied up to 25mm during the course of the experiments. This system was stirred using a single air jet, with a flowrate ranging from 7.66×10^{-6} to 4.17×10^{-4}m^3/sec, issuing upward from the bottom surface of the vessel. Measurements of mixing time and entrainment of oil in the water were carried out The following sections will describe the equipment developed for these purposes.

2.3 Measurement of Mixing Behaviour

During studies of mixing behaviour by other investigators, many techniques have been developed for measuring the mixing time in vessels Bath homogenization is appraised by monitoring the disperison of a tracer material, typically a liquid, which is injected into the bath Each of the measurement techniques developed exploits a physical or chemical difference between the bulk fluid being stirred and the injected fluid. By monitoring the variation of the chosen property at one or more locations within the bath, it is possible to determine when the measured quantity ceases to change. At this point the bath is considered to be completely mixed The time for complete mixing is difficult to measure, though, because the homogenization is approached asymptotically and not suddenly. Therefore, the mixing time is defined as the time required for the measured property change to remain within a specified margin of the final total change In this study a $\pm$ 5% band was selected. This concept is depicted in Figure 2.1, which shows a normalized property change as a function of time.

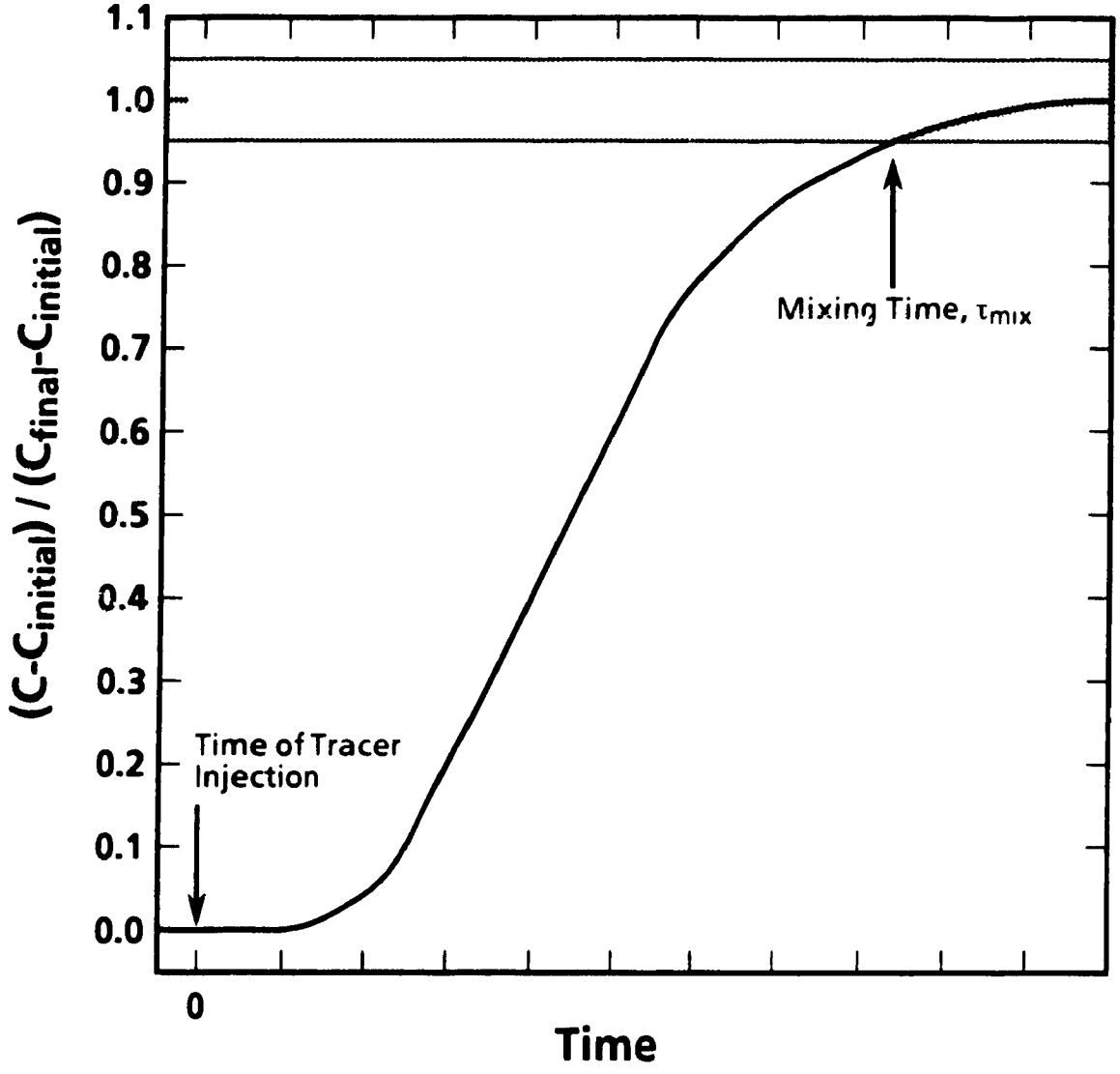

Figure 2.1 Schematic Representation of Mixing Time Response Curve

2.3.1 Previously Developed Techniques

Some of the more commonly used systems for measuring tracer dispersion monitor properties such as:[40]

a) temperature:

The tracer material, typically the same as the bulk fluid, is at a different temperture than the bulk. Mixing is followed by monitoring the bulk temperature with a thermocouple.

b) electrical conductivity:

An electrically conductive liquid (eg. potassium chloride solution or concentrated hydrochloric acid) is injected into a less conductive bath (eg. water) and the electrical conductivity at various locations within the bulk is monitored.

c) index of refraction:

This technique requires a relatively large volume of injected liquid, with a refractive index different from that of the bulk liquid, to ensure accurate measurements. As the two liquids blend, the local refractive index of the bath changes. This technique is known as the Schlieren method.

d) pH-value and chemical decolourization:

Monitoring of the redox potential of the bath using a pH meter, after the addition of an acid, is similar to the electrical conductivity method. When using decolourization, a soluble pH indicator is mixed into the bath prior to the addition of the tracer, typically an acid. As the tracer disperses, the redox potential of the bath changes and the liquid undergoes a colour change; usually it becomes colourless. The time required for complete colour change, as detected visually, can be measured using a stop watch.

e) dye tracer injection:

a small volume of concentrated dye is injected into the bath and the distribution of the color concentration is monitored either visually or photoelectrically.

The majority of these techniques, including the commonly used conductivity method, measure the local mixing behaviour since a small sensor

is located at one position in the bath. Many studies in which local mixing was measured concluded that when employing such techniques the position of both the sensor and the tracer addition are critical on the mixing time measured.[9,25,41] Using a three dimensional mathematical model for gas stirred systems, Joo and Guthrie demonstrated a dramatic change in mixing behaviour during the chemical homogenization of alloy additions when the injection position of the alloy is changed only slightly from a central position.[42] Therefore, unless the different investigators use identical techniques in physical modelling studies, it is difficult to directly compare their results. Even the accurate scale-up of results from a model may be questionable. The local mixing time is useful, however, in analyzing the effects of changes in operating parameters on general qualitative behaviours within the scope of a given study.

Due to the non-intrusive nature of the decolourization and dye injection techniques, they typically do not measure mixing at a single given location. Instead, global mixing throughout the vessel is assessed. Therefore, sensor location is no longer as sensitive since a larger volume, if not the entire bath, is being monitored. However, the location of the tracer injection is still important.

2.3.2 Systems Used in Study

Due to its ease of application, the measurement of electrical conductivity is the most widely used technique when studying homogenization. Another advantage is the possibility of multiple experiments in the same initial volume of water before the accuracy of the measurements diminishes as a result of a high electrolyte concentration. However, this technique was not feasible in this study due to the presence of the oil phase. At low stirring energies, no problems were encountered, but when the bath was highly agitated significant entrainment of the oil occurred deep within the bath. When the oil droplets came into contact with the electrodes of the sensor the measured response deteriorated quickly and became erratic. Therefore, another technique was needed, one which was not affected by the oil phase. The dye injection technique was chosen since photoelectric measurements could be carried out without submerging the

sensor in the liquids. The dye also allowed the visualization of the flow pattern of the bulk liquid during its first circulation

The monitoring system developed for this study consisted of two CdS photoresistors (Figure 2.2), approximately 10mm in diameter, placed on the outer surface of the square plexiglass tank built around the cylindrical model The sensors, symmetrically arranged on the front surface, were located at approximately the mid-radius position and 50mm below the oil/water interface. Two sensors were used in order to monitor the evenness of the dye dispersion on opposite halves of the vessel. Figure 2.3 shows a schematic of the layout of the apparatus used for these measurements. A 250W light source was placed on the opposite side of the tank from the sensors A diffusion plated was inserted between the light source and the tank to provide an even distribution of light across the face of the tank In order to limit the amount of light transmitted to the sensors, a black plate was then placed between the diffusion plate and the tank. Two holes, which were aligned with the sensors, were made in this plate to allow light transmission In this manner, two beams of light passed through the vessel instead of the entire volume being illuminated. Finally, the space between the cylindrical and square tanks was filled with water to reduce the light refraction at the curved surfaces.

After the bath had been stirred for a sufficient length of time to establish a steady fluid motion, one milliliter of water soluble dye was injected into the center of the rising two phase plume using a lance submerged to a depth of 30 to 40mm below the oil/water interface As the dye dispersed through the water, the amount of light transmitted through the narrow light beams to the sensors was diminished. The voltage output from the photoresistors, which were powered by a 5V DC source, then increased and the change was monitored using a digital chart recorder The data was also transferred to a host computer for storage and future analysis The amount of dye used was selected so as to not saturate the voltage readings. Figure 2.4 is the result of calibration tests which showed that with 2ml of dye the change in the recorded voltage reached a plateau, whereas 1ml resulted in a voltage response in the most sensitive portion of the calibration curve.

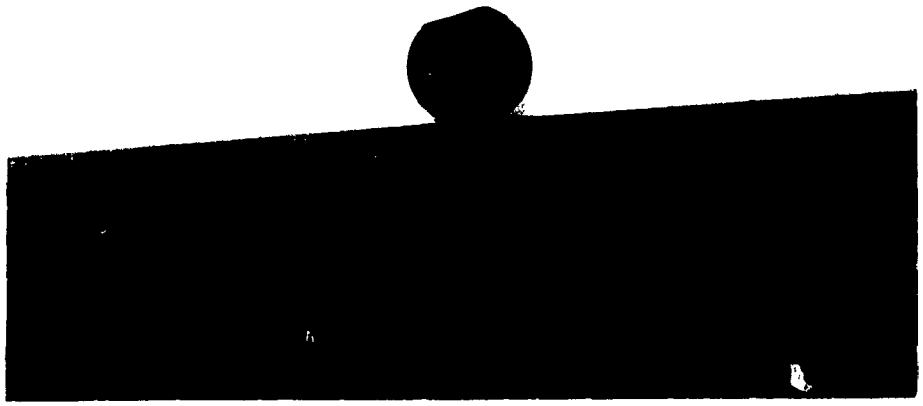

Figure 2 2 Photograph of the CdS Optical Sensor for Monitoring the Mixing Behaviour

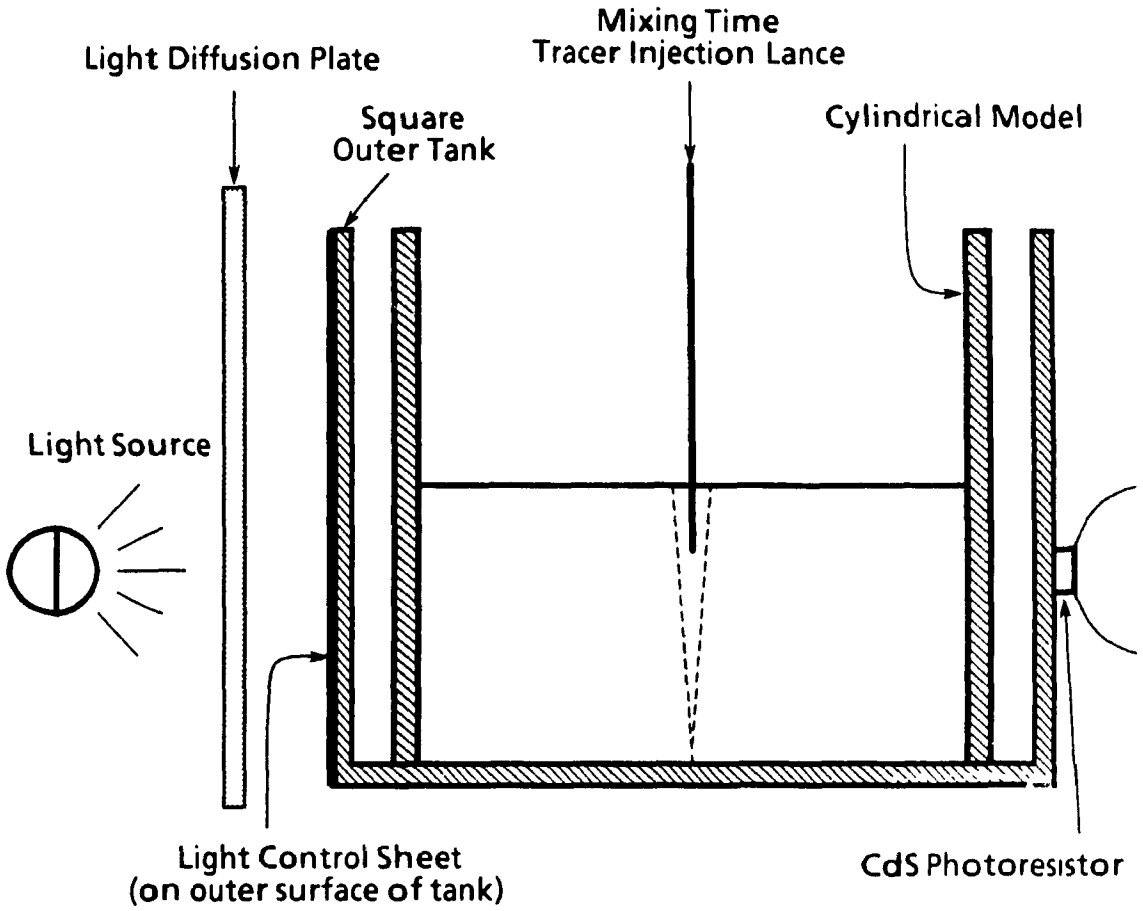

Figure 2.3 Schematic of Experimental Apparatus Indicating Mixing Time Sensor Configuration

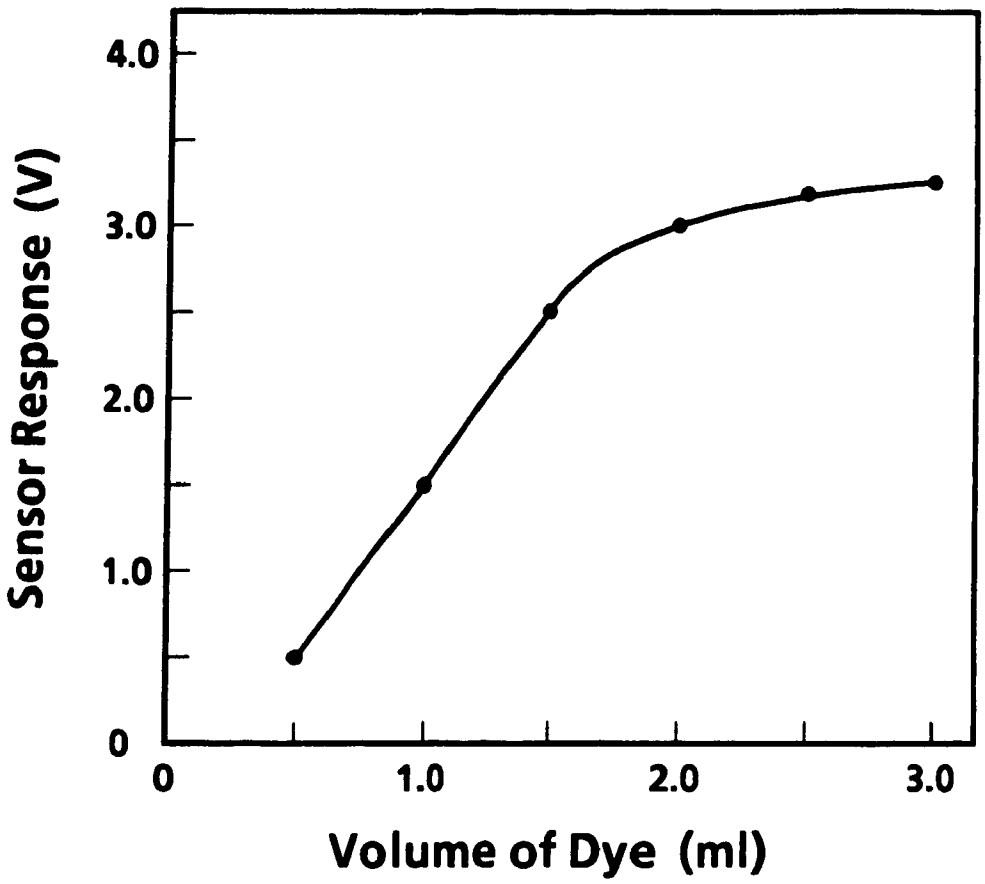

Figure 2.4 Calibration Curve of Voltage Response with Dye Injection

Other investigators have used photoelectric techniques for monitoring mixing.[43] However, their studies were mostly concerned with channel reactors or other flow-through vessels. This study was concerned with mixing within a closed system and the reliability of the dye injection technique has never been analyzed under such conditions. With the volume of liquid in the detection zone being greater than for localized monitoring sensors, it was expected that the mixing times may be as much as 3 to 6 times shorter than if measured by electrical conductivity.[44] To test the reliability of the photoelectric system, experiments were performed in which no oil was present, leaving the surface of the water free. Mixing times were measured using both the dye injection and electrical conductivity techniques. The conductivity probe was constructed of two 1.0mm diameter stainless steel electrodes, with an exposed length of 20mm and separated a distance of 4mm. The probe was positioned at the mid-radius, half-depth position in the bath so as to measure within the zone monitored by the optical sensor. Two milliliters of 2M KCl solution was injected into the center of the plume, in the same manner as the dye. Typical response curves from the two sensors, for experiments involving a gas flowrate of $3.93 \times 10^{-5} m^3/sec$, are compared in Figure 2.5. The two apparent mixing behaviours were similar, but the dye injection technique did indeed generate shorter values for the time of homogenization of the injected tracer.

The measure of light transmitted through the water decreases as the dye mixes in the tank. Therefore, an overall nature of the mixing behaviour is being monitored using this technique, as opposed to the localized behaviour detected by the conductivity probe. In this manner, this device may be considered to be an averaging device of all the localized behaviours present in the beam of light passing through the model.

Figure 2.6 shows the variation of mixing time with gas injection rate, as determined by the two sensors. As expected, the local mixing behaviour is slower than the more global measurement. More importantly, the variation of mixing time with gas flowrate is virtually identical for the two systems. Therefore, it would appear that the dye tracer system is reliable in demonstrating the mixing behaviour, as long as one remembers that the

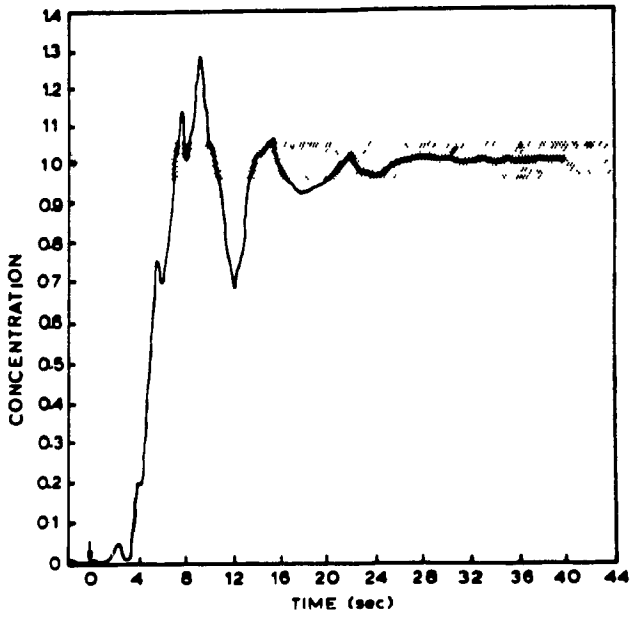

a. Electrical Conductivity Measurment

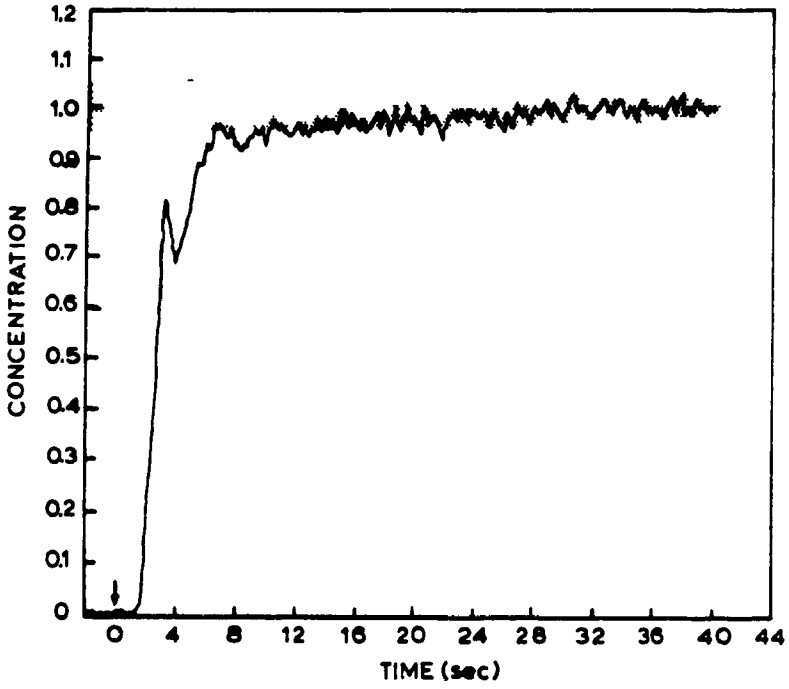

b. Dye Injection Tracing

Figure 2.5 Mixing Time Response Curves using Two Detection Techniques

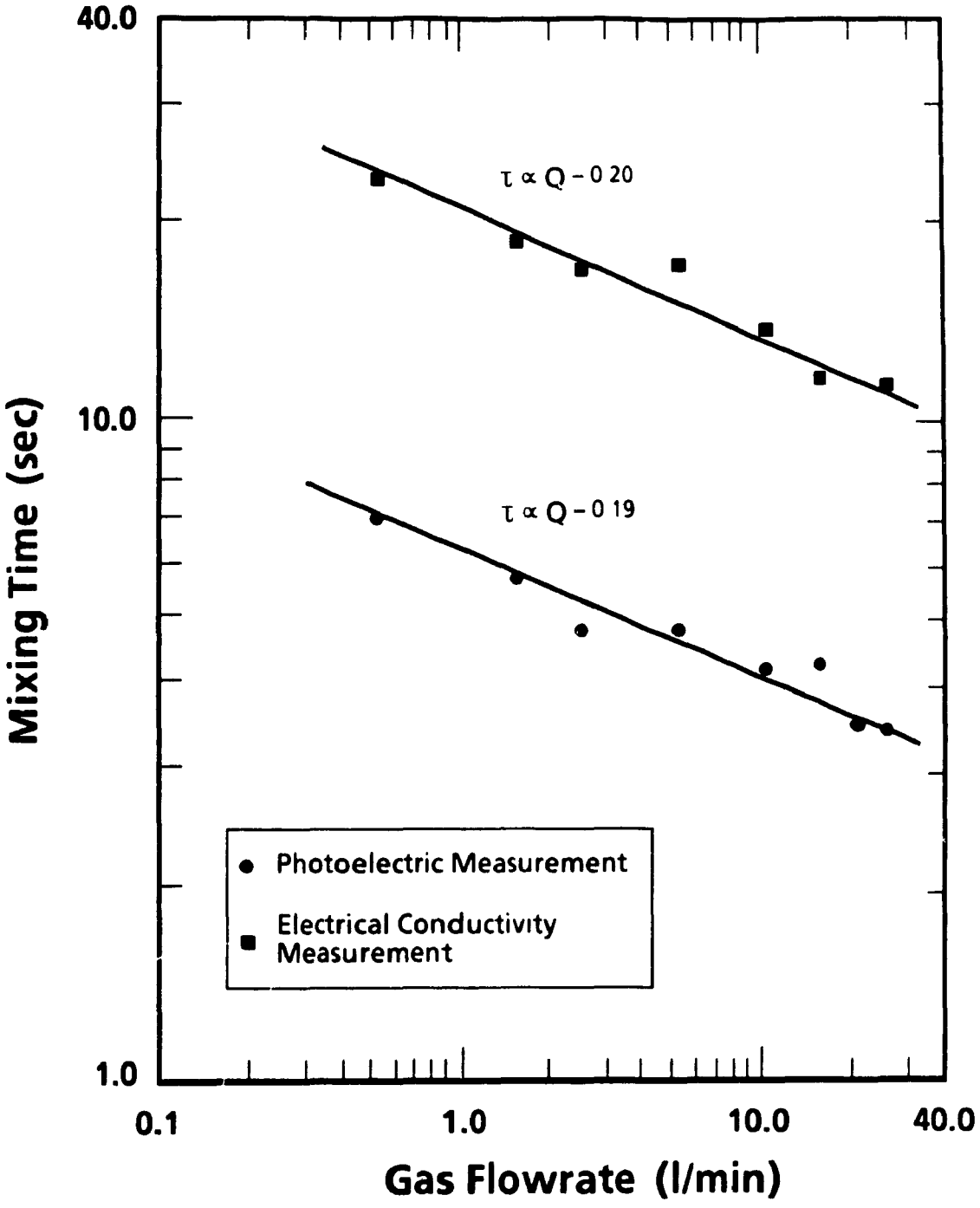

Figure 2.6 Comparison of Mixing Time Data for Two Measurement Techniques

magnitude of the mixing times are at least 3 times as low as for other techniques, which agrees with the comments made previously.

2.4 Measurement of Entrainment Behaviour

In previous studies of entrainment in agitated liquid-liquid systems, two methods of analyzing the size and number of entrained droplets have been typically employed. The simplest involves the extraction of a small sample of fluid from the vessel using a vacuum device.[45] The sample containing entrained droplets is then held static in a long clear tube, or other holding system and photographs are taken. The photographs are subsequently analyzed to determine droplet sizes. The other method involves the use of electronic detection and counting devices, such as the Coulter counter, for the continuous analysis of extracted samples.[46] Tanaka developed a slightly different electronic device for in-situ measurements of entrained oil droplets in water [33] The sensor contained two closely spaced platinum electrodes positioned in a sampling tube. Fluid, containing entrained oil droplets, was continuously drawn from the model through the tube and when the entrained oil droplets passed between the two wires a detectable voltage response was generated. That technique was attempted in this study, but very erratic voltage responses were recorded as the wires became increasingly contaminated by the oil, in the same manner as for the submerged mixing time sensors. Also, the system was only capable of indicating the presence of a phase which was not the same as the bulk phase. In strongly agitated gas stirred systems the detected phase could be either entrained oil or entrained air bubbles, and therefore it is important to distinguish between all three phases involved.

For this study another in-situ system was developed which was not hampered by either of these problems. The system was based upon the detection of the difference in the index of refraction of the three phases involved: oil, water and air. The values for air, water and 200 Fluid are 1.00, 1.33 and 1.40, respectively. A peristaltic pump continuously drew a sample of the bulk fluid at a constant rate through a 1.19mm internal diameter transparent flexible tube. The tubing was inserted into a sensor assembly containing a light emitting diode (LED) and a phototransistor. The sensor

was located between the vessel and the pump to ensure that entrained air bubbles and oil droplets were not broken as a result of passing through the pump. As the different phases passed between the photoelectric devices a different voltage output was registered for the corresponding phase, depending upon its index of refraction A voltage reading of 3.0V was recorded for water while oil and air had readings of 2.5 and 1 0V, respectively A bell shaped nozzle was attached to the input end of the sampling tube to facilitate easy entrapment and extraction of oil droplets from the bath. The fluid was withdrawn at a rate of between 40 and 60ml/min. The rate was varied in an attempt to withdraw the fluid at the same velocity as the surrounding bath in order to not bias the extraction of droplets. Entrainment behaviour was monitored at nine locations in the bath, which are indicated in Figure 2.7.

2.4.1 Entrainment Sensor

Presented in Figure 2.8 are a photograph of the photoelectric device used and a schematic of the complete sensor assembly. Installed in the space between the LED and the phototransistor was a hollow stainless steel holder. In order to allow light from the LED to pass through the transparent sample tube, which was inserted through the rigid steel holder, a slot 1 6mm wide was cut in the holder Directly opposite this slot was another slot, 0.5mm wide, which allowed light to pass to the transistor. The slot on the side of the LED was made wide to allow sufficient light to enter the clear tube. The other slot, however, had to be maintained narrow in order to enhance the accuracy in detecting the starting and trailing ends of the entrained droplet passing through the sensor, yet wide enough to allow sufficient light transmission for adequate accuracy in the output.

2.4.2 Electronics used for Entrainment Detection

The counting of entrained droplets was accomplished by passing the voltage response from the sensor through an electron circuit containing a voltage peak height analyzer. This is the same equipment used by Nakajima

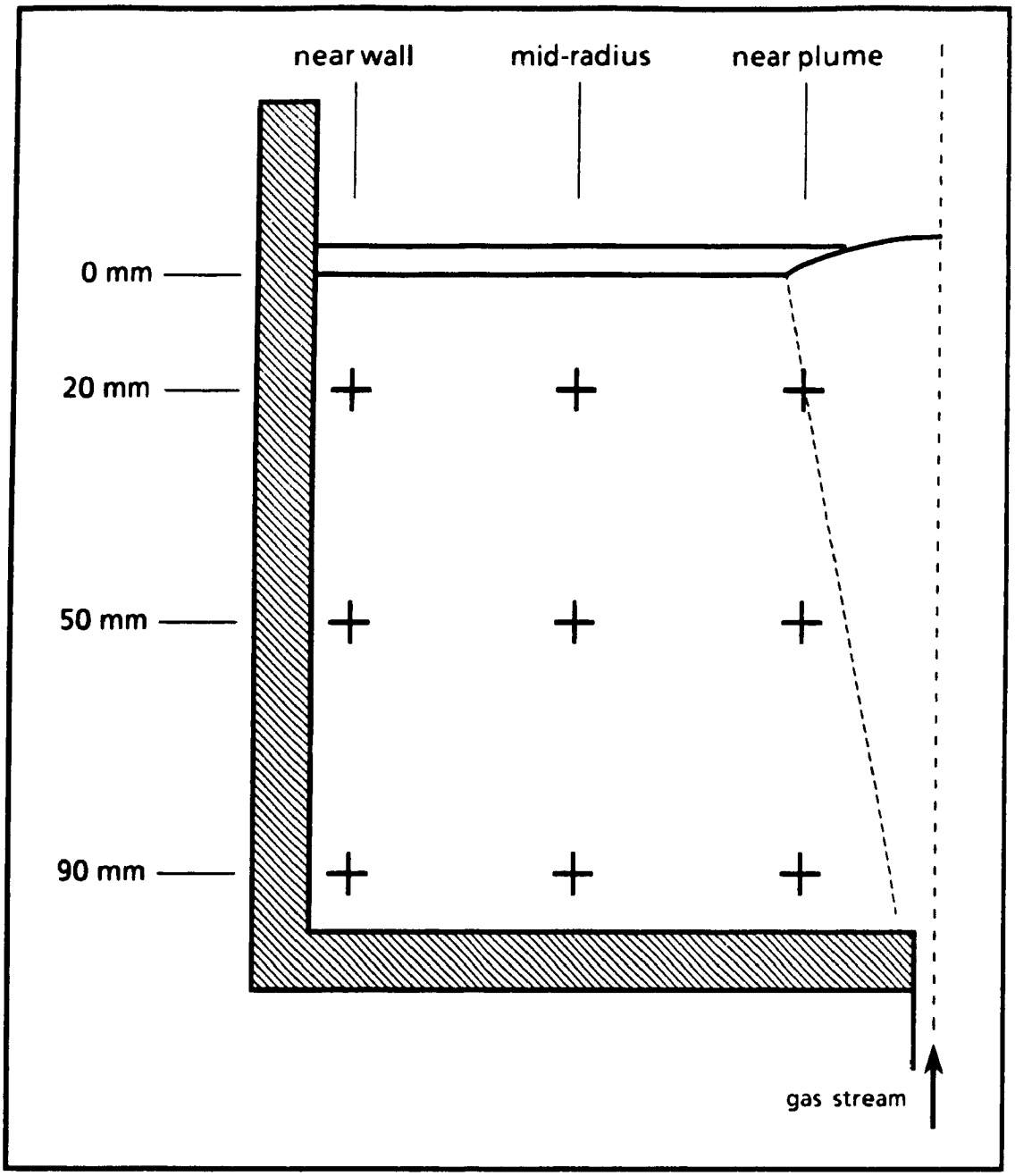

Figure 2.7. Location of Entrainment Sampling Points

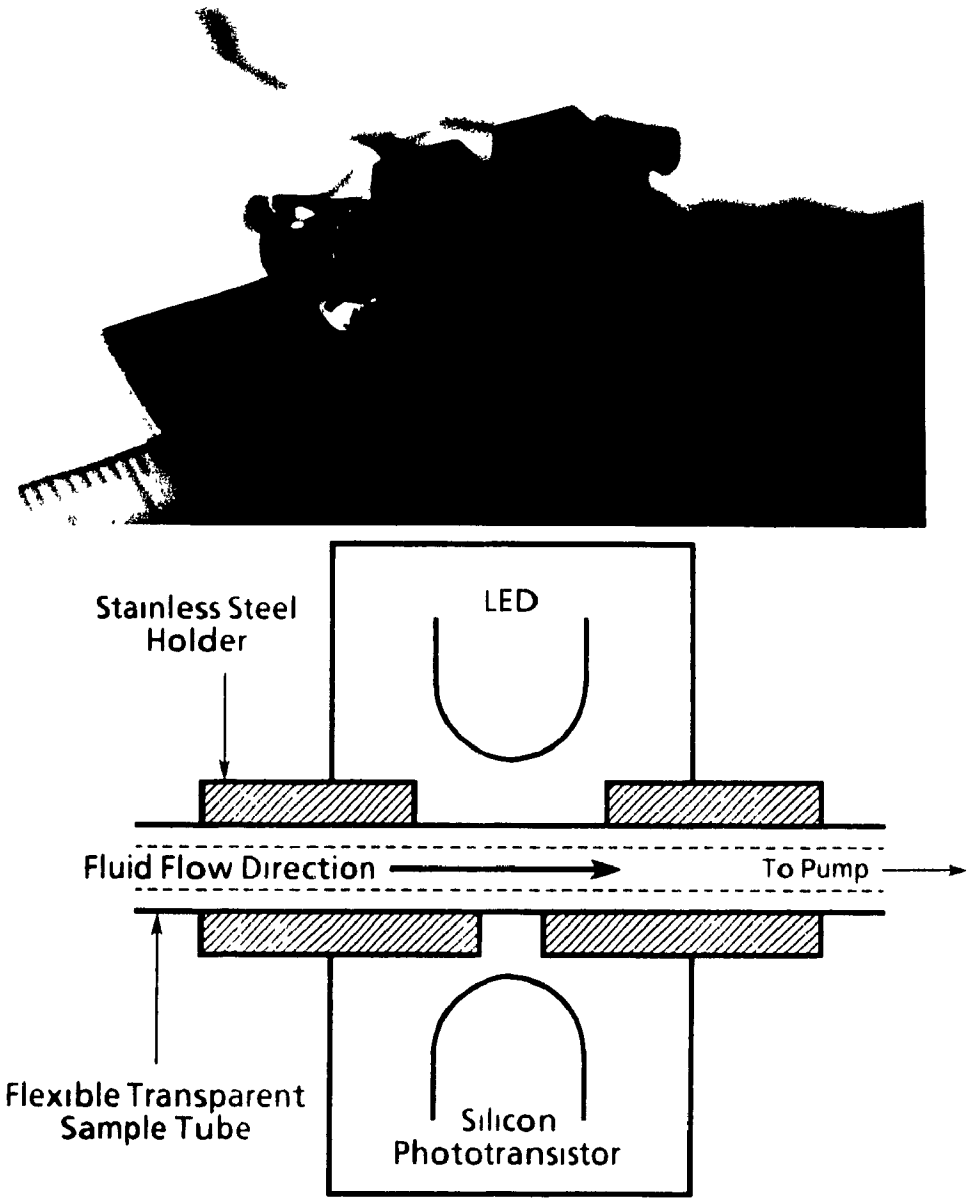

Tubing:	1.19mm ID
	1.70mm OD
LED Slot:	1.6mm
Photosensor Slot:	0.5mm

Figure 2.8 Photograph and Schematic Representation of Entrainment Sensor

for the detection of non-metallic inclusions in steel. A detailed description of the equipment can be found elsewhere.[47] The system is capable of counting voltage peaks of variable height, with respect to a steady baseline voltage, supplied to a digital oscilloscope. From the voltages listed above, if water is the bulk fluid, the baseline would be set at 3.0V and the passage of either oil or air through the sensor would produce a voltage peak. However, the counting system is not capable of distinguishing between the two entrained phases and would give a total count of entrained oil and air. Therefore, a pre-processing circuit was built to allow the electronic identification of the two phases.

The pre-processing circuit was used to divide the single channel output from the sensor into a dual channel output. The response of each channel was either 0 or 5 volts, depending upon the settings of the electronic voltage triggers contained in the circuit. A schematic of the circuit is presented in Figure 2 9. It contained two independent variable voltage triggers comprised of variable resistors. When the voltage from the sensor is at 3V both triggers would open and the readings from the two output channels would both be 5V (see Figure 2.10). When the input voltage drops below the set point of the first trigger, which was set at 2.8V, the first channel would be turned off, but the second remains open. The output of the first channel would be 0V while the second remains at 5V. When the input voltage is below the second trigger set point of 2 3V both triggers would close and both outputs would read 0V. By monitoring the two output channels with an oscilloscope, the phase passing through the sensor can be determined; both channels at the 5V baseline indicates water, a voltage of zero on one channel and five on the other indicates a passing oil droplet, and a zero voltage reading on both channels indicates an air bubble. By counting the inverted peaks on each channel, the number of air and oil droplets entrained in the bulk fluid can be determined.

As a result of the configuration of the preprocessing unit, the output voltage peaks tended to be in a square wave form, as indicated in Figure 2.11, which schematically shows the passing of an oil drop closely followed by an air bubble. The length of a peak on the oscilloscope corresponds to the elapsed time of the entrained droplet passing through the sensing zone.

Hence, the accuracy in determining the starting and trailing ends of the droplet tube is important. An estimation of the size of the entrained phase can be made by using the elapsed detection time and the velocity of the fluid through the collection tube. It is important to note that if the droplet diameter was greater than the tube diameter (i.e >1.19mm) it would become elongated in the tube. This elongation must be considered in the estimation of droplet size Example calculations for droplet determination are presented in Appendix A. An estimation of the size distribution of entrained oil droplets was made from several of the elapsed sensing times measured from the oscilloscope responses. A continuous monitoring of droplet size was not attempted.

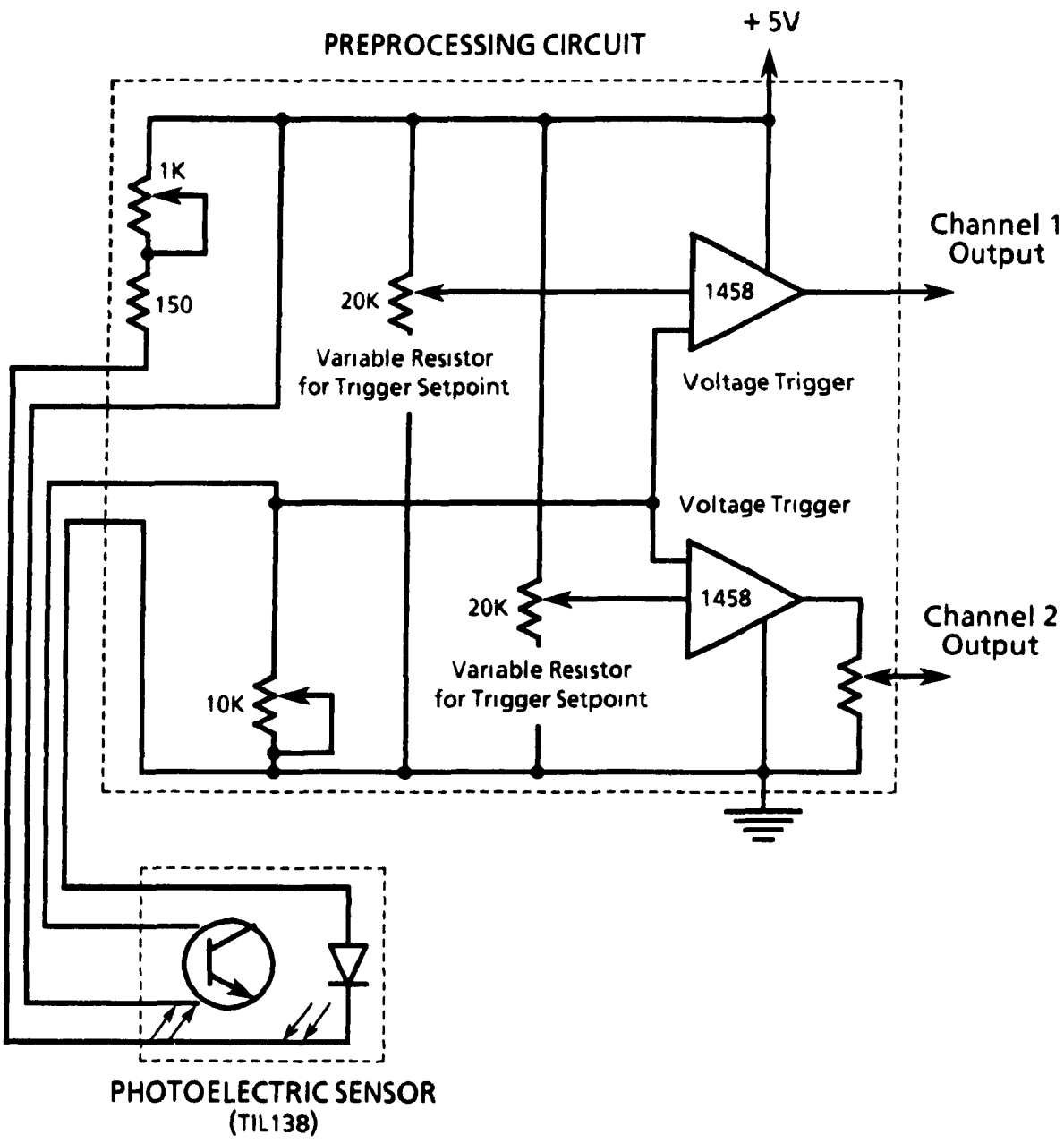

Figure 2.9 Circuit Diagram for the Pre-Processing Circuit and Entrainment Sensor

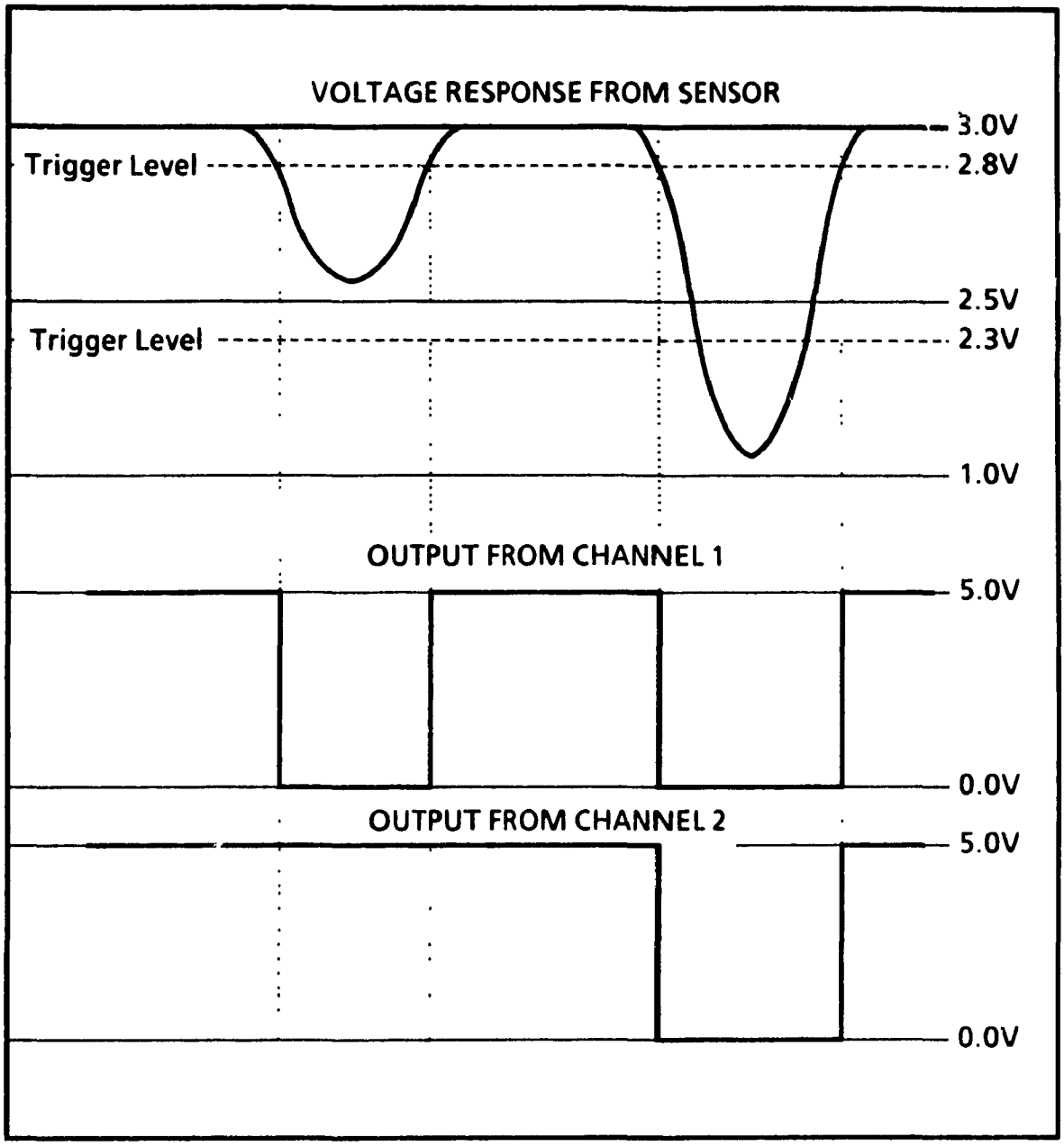

Figure 2.10 Triggered Response of Oscilloscope Output for Different Entrainment Sensor Responses

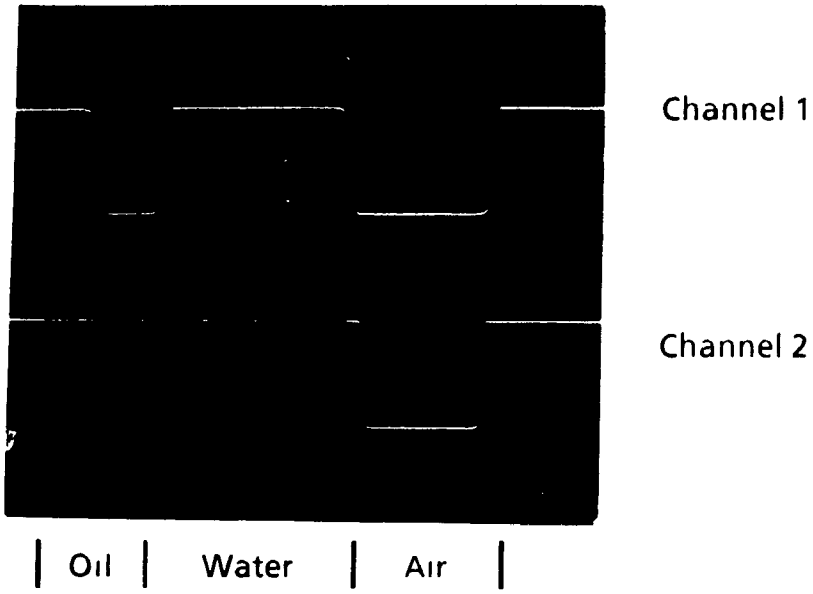

Figure 2 11 Photograph of the Oscilloscope Response with the Passage of an air bubble and oil droplet

3 RESULTS AND DISCUSSION

3.1 Mixing Behaviour

The mixing behaviour of a gas stirred system was characterized in terms of the mixing time of the bulk liquid as a function of the gas flowrate and the thickness, and viscosity, of an overlying oil layer. Visualization of the fluid flow patterns in the bulk liquid, which govern the mixing behaviour, was also attempted. In order to understand the influence of the oil layer on the mixing behaviour, comparisons were made with an oil-free system and a system containing a rigid wooden plate floating on the bath surface

3.1.1 Flow Visualization

Very fine aluminum flakes were added to the agitated water while the tank was illuminated by a slot lamp installed along its central plane. In this manner, only the flakes tracing out the flow pattern in the narrow plane of light were visible producing a two-dimensional image. All photographs of the flow field presented in this study show one half of the vessel with the plume to the right and the tank wall to the left. Figure 3.1a shows the general counterclockwise recirculatory flow in the left side of the oil-free bath generated by the injected gas. In this case, the gas flowrate was 1.42l/min. The aluminum powder streaks reveal the presence of the center of the recirculation loop near the vessel wall at approximately half depth, and the flow of liquid into the two-phase plume region.

Rigid versus free surface conditions for lower phase gas stirred systems

Figures 3.1b, c and d show the flow patterns for the same gas flowrate but with the water covered by: a) a 10mm thick wooden plate, b) a 10mm and 3) a 25mm oil layer, respectively. It should be noted that a hole, the diameter of the exposed plume eye, was cut into the center of the wooden plate to allow the injected gas to freely escape without becoming entrapped under the plate. For a low gas flowrate, the presence of a thin upper layer, either oil or wood, does not appear to significantly influence the overall flow pattern. The same conclusion was made by Mazumdar, Nakajima and

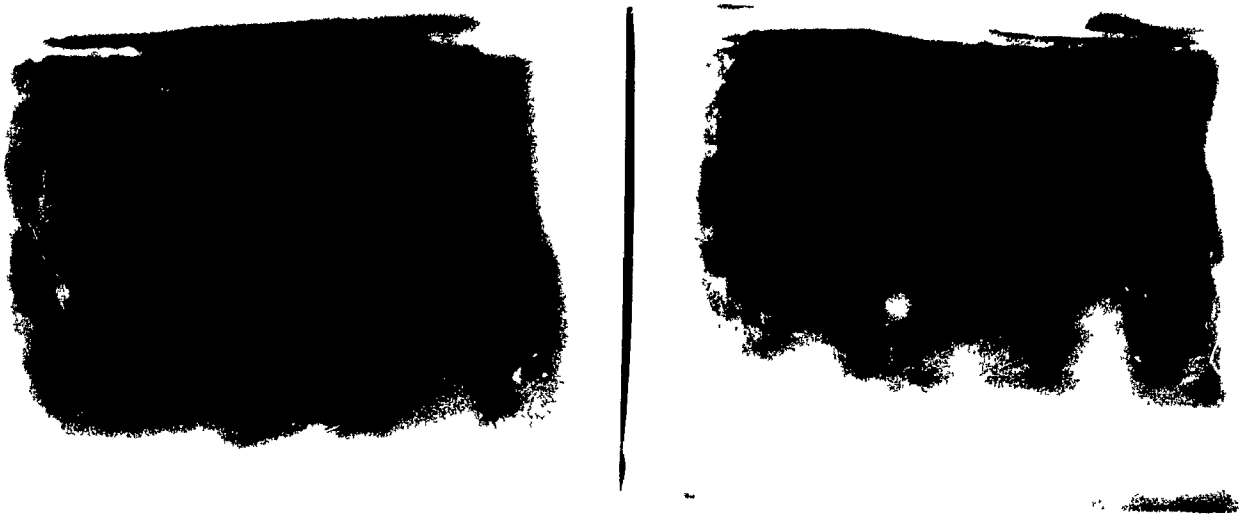

(a) Free Surface

(b) Wooden Plate

(c) 10mm Oil Layer

(d) 25mm Oil Layer

Figure 3.1 Flow Visualization in the Water Model for Different Test Conditions and with an air flow of 1.4 l/min.

Guthrie[29] who used a grid of silk threads to visualize the flow pattern. However, the authors concluded that the presence of a second phase results in a slight alteration in the velocity profile at the interface between the upper and lower liquids.

In the system containing only water, the velocity at the free surface is strictly horizontal, as was described in section 1.2.1. The presence of the second phase creates a slight vertical component in the velocity in the water at the interface between the water and the overlying material. A closer comparison of Figure 3.1a and c reveals that the oil layer does produce a slightly different profile in the upper region. The eye of the rotation moves lower down and further from the side wall in the presence of an upper layer, as compared to the oil-free case. In the upper region, directly below the liquid-liquid interface, the fluid appeared to be more turbulent, with small eddies present.

Effect of upper phase thickness

A substantial change in the flow field profile did occur when the thickness of the oil layer was increased to 25mm (figure 3 1d). For low gas flowrates, the rotational direction of the recirculatory flow became reversed, as compared to the thin layer. In addition, the average fluid velocity was greatly reduced as indicated by the relatively low concentration of entrained aluminum flakes. A schematic of the flow field shows that for thin oil layers the liquid from the plume, and in the interface region, is directed radially outwards with a slight downward component, as mentioned by Mazumdar et al. (see Figure 3.2) As the upper layer becomes thicker, the downward component is increased due to an increased redirective influence of the interface between the oil layer and the plume. The downward flow of water from the oil/plume interface eventually resulted in the formation of a two-zone pattern with the recirculatory flow in the zones moving in opposite directions. The vertical component of velocity continues to increase in the plume/oil region as the thickness of the upper layer was further increased until complete downward redirection occurs. The change in the flow pattern as a result of an increase in the thickness of the upper layer is demonstrated in Figures 3.2a and 3.2b. This was the case for the system containing a 25mm

thick oil layer, depicted in Figure 3.1d. Viscous and momentum forces are then responsible for the generation of a slow recirculatory flow in the bulk liquid in the opposite rotational direction to the tight recirculatory flow near the plume.

Role of gas flowrate

The completely vertical redirection of liquid by the oil layer was only possible when the energy input by the injected gas was not sufficient to cause the coherent oil layer to break into droplets. At the low flowrate, the oil in the plume region was displaced, but otherwise the integrity of the layer was maintained. When the air flowrate was increased to 5l/min, no qualitative changes occurred in the flow patterns. However, beyond this value, it was noted that the energy input attained a level sufficient to cause a substantial break up of the oil layer into a layer of large oil spheres, resembling a coarse emulsion. Figures 3.3a, b, c and d show the flow patterns for the free surface, wood covered, thin oil layer and thick oil layer systems, respectively, for a gas flowrate of 15l/min.

For the oil-free system, the pattern is qualitatively similar to that for the low flowrate case. Increased turbulence in the upper region was noted as a result of bath oscillations and splashing. This simple recirculation pattern was seen over the entire range of gas flowrates used in this study. Even though the recirculation pattern in the vertical plane was consistent, changes to the movement of the plume did occur in the oil-free system as the gas flowrate was increased. Initially, greater gas injection rates resulted in an increase in the level of splashing and oscillation of the free surface of the water. Further increases in the flowrate resulted in the onset of plume rotation about the central axis of the cylindrical vessel. This swirling action of the plume could be envisaged as generating a conical shape in the bath, with the tuyere being at the tip of the cone. Krishna Murthy et al.[48] also studied this behaviour of the plume and reported that the ability of a plume to rotate is greater for shallow baths, such as used in this study, than for deeper baths.

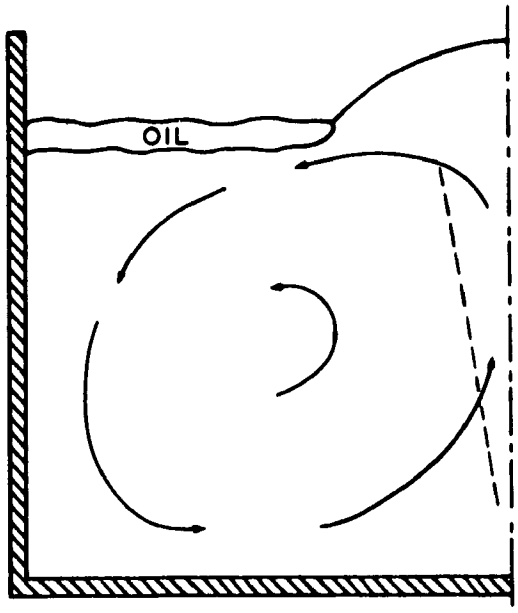

(a) Thin Upper Layer

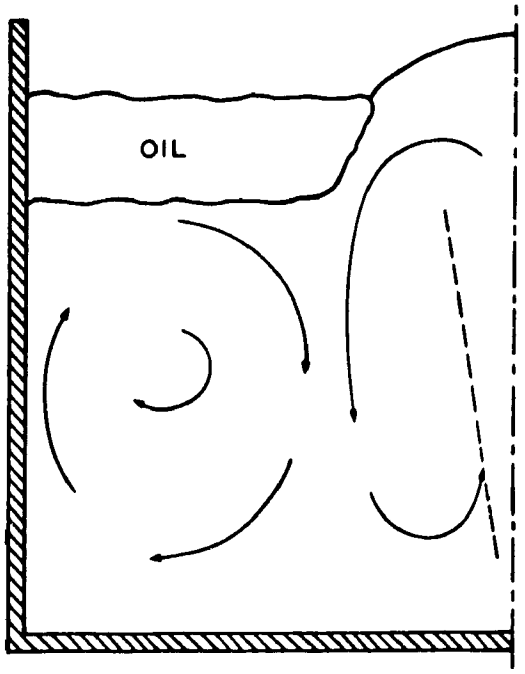

(b) Thick Upper Layer

Figure 3.2 Schematic representations of the bulk fluid motion in gas stirred vessel with varying thickness of a less dense upper layer.

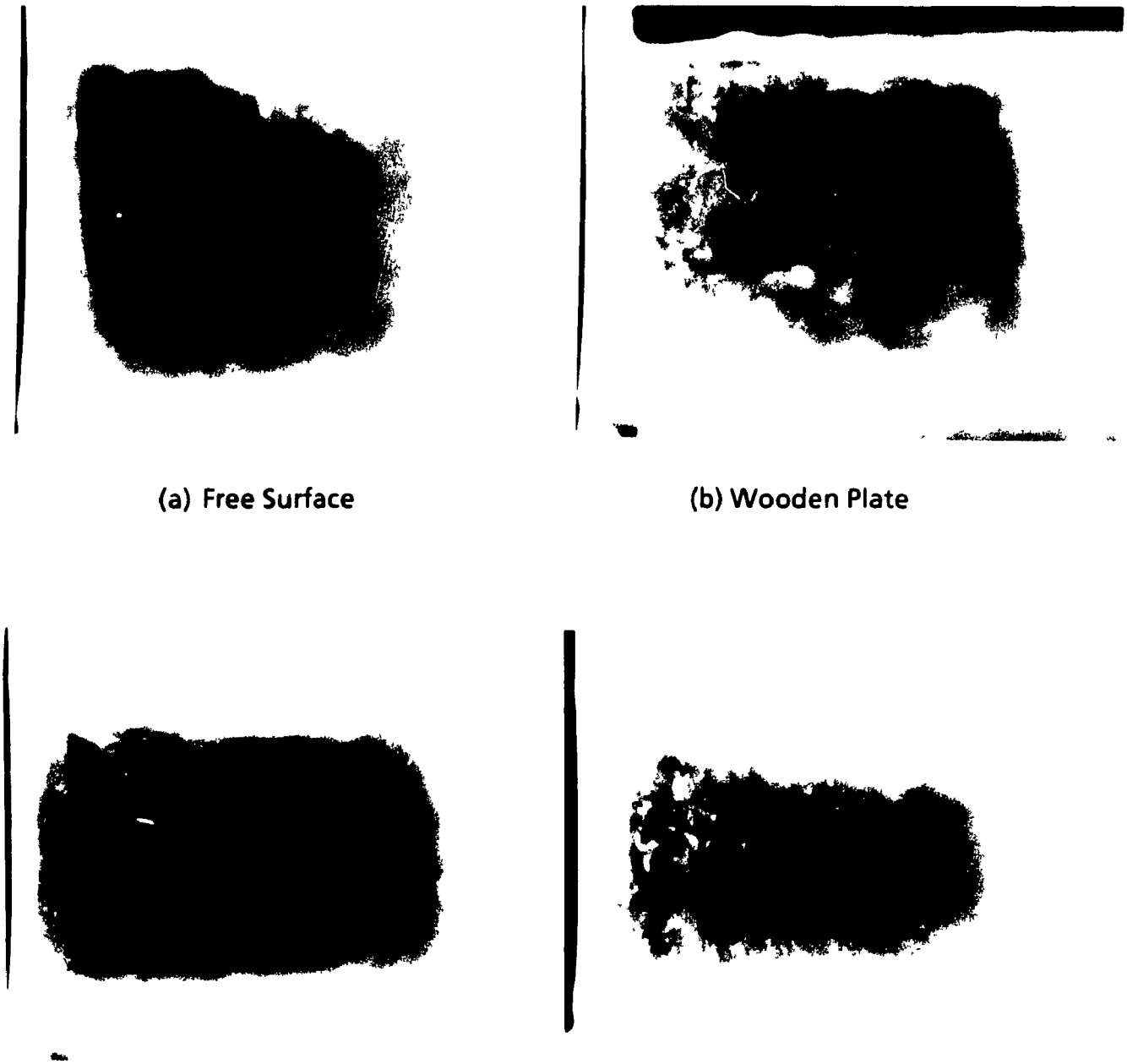

(a) Free Surface

(b) Wooden Plate

(c) 10mm Oil Layer

(d) 25mm Oil Layer

Figure 3.3. Flow Visualization in the Water Model for Different Test Conditions and with an air flow of 15.0 l/min.

For the wood covered system, however, a notable change occurred. Although the recirculatory pattern was still present, the level of turbulence in the bath appears to have increased dramatically, particularly in the near-wall region below the wooden block. It would appear that the increased input energy could not be dissipated by bath oscillation, as in the free surface case, and therefore was responsible for increasing the overall bath turbulence below the wood. Similar results were found for the bath covered by a thin oil layer (figure 3.3c). The turbulence appears to be slightly lower since some energy is dissipated through a distortion of the oil/water interface, while the free surface of the oil remained relatively calm.

In the presence of a wood surface, or a second liquid layer of higher viscosity than the bath, the rotation of the plume noted at higher gas flowrates for the single fluid tests was not noticed. Krishna Murthy et al reported that the presence of a spout breaker, which reduced the oscillations of the bath surface, extended the range of the gas flowrate before plume rotation occurred. The cylindrical spout breaker in their study was not situated on the surface of the bath but rather was held a distance of 25mm above the surface. Therefore, it would appear that the presence of a second phase across the sruface of the bath results in a reduction of the oscillations of the bath surface, which appears to eliminate plume rotation

The results of the thick oil layer system showed the greatest change as the flowrate was increased past 5l/min. As mentioned, beyond this level sufficient energy was available to break up the oil layer. Since the integrity of the oil layer was degraded, the redirective capability of the oil/plume interface was also greatly reduced. As a result, the direction of recirculation was changed to match that of the other systems which contained no oil, or a thin oil layer. Also, as the oil layer broke up into a collection of droplets, the thickness of the upper layer increased.

Conclusions

The visualization experiments have given some insight into the general flow patterns in the bulk liquid, which controls the rate of chemical and thermal homogenization. These results will be used to help explain the

mixing behaviours observed and which are discussed in the following sections.

3.1.2 Mixing Time Versus Gas Flowrate

To start the investigation of how operating parameters affect mixing behaviour, the influence of the input gas flowrate on the mixing time was considered. As was discussed in chapter 1, a simple power law relationship has been found to exist for systems containing one liquid, or for systems containing two liquids over a narrow range of flowrates. As a standard for comparison, this relationship was studied in the present model containing only water for the series of flowrates outlined in Table 2.2. The results are presented in Figure 2.2. As is shown, a single relationship, in the form of equation 1.4, does exist over the entire range of flowrates with a value of -0.19 for the flowrate exponent, n. The form of the relationship agrees with other investigators but the value of n is at the lower end of the spectrum of values determined in other studies. The value is close to that of Helle[21] who used a model with an aspect ratio similar to the current system, which was 0.33.

Another standard for comparison was a system containing a wooden plate floating freely on the surface of the water. The results for this configuration are presented in Figure 3.4. It can be clearly seen that one expression no longer describes the mixing behaviour of a covered system over a wide range of gas flowrates. The mixing process seems to be greatly enhanced at higher flowrates as compared to the more gently stirred systems.

Before any further analyses were undertaken, the behaviour described in figure 3.4 was verified using the electrical conductivity technique, as was previously done for the free surface configuration. The verification was deemed necessary to confirm that this trend was not a result of some phenomenon of the photoelectric technique employed. Conductivity measurements were made at two locations in the bath; near the wall and at midradius. Both locations were at the half depth position. The results of the two measurements were virtually identical, with the times measured near the

wall being slightly longer. The results of the conductivity measurements at the mid-radius and those of the photoelectric technique are compared in Figure 3.5. The dye injection technique produced much shorter times, but more importantly, the two techniques both show the sudden change in mixing behaviour at a gas flowrate of 10l/min. Therefore, the trend presented in Figure 3.4 would appear to be a result of a change in the mixing process at higher flowrates and not a result of the measurement process

Figure 3.6 shows the mixing results for systems containing oil layers of 10 and 25mm thickness, respectively The oil used had a dynamic viscosity of 5×10^{-5} m²/s. Again, both lines show the sudden change in the value of the gas flowrate exponent from an initial value of -0.2 to -0.30 to a value of -0.8 to -1.1. These values are similar to the values of -0.13 and -1.0 determined for the tests involving the floating wooden block. Experiments involving the lower viscosity oil were also performed and the values of n determined for these tests, as well as those for the oil-free, wooden plate, and higher viscosity oil systems are presented in Table 3.1 From the values listed in the table, the flowrate exponent increases slightly as the thickness of the oil layer is increased. For all experiments involving an oil layer, regardless of its thickness or viscosity, the flowrate at which the value of n changes was approximately 5l/min.

The seemingly sudden increase in the influence of the input gas flowrate on homogenization is believed to be related to a change in the state of the flow pattern in the water. As was stated in chapter 1, mixing is governed by convective and diffusive mass transport. The rate of convective transport is linked to the velocity of the fluid, which in turn is controlled by the entrainment of liquid into the central two-phase plume and the size of the convection loop. Diffusion of a tracer through the bath is strongly influenced by the level of turbulence within the fluid Chemical homogenization in a vessel in which the level of turbulence is low would require the completion of a greater number of convective loops, and therefore longer times, than if the diffusive component were greater. Therefore, a change in either of these transport processes may be responsible for the noted shift in the value of the flowrate exponent.

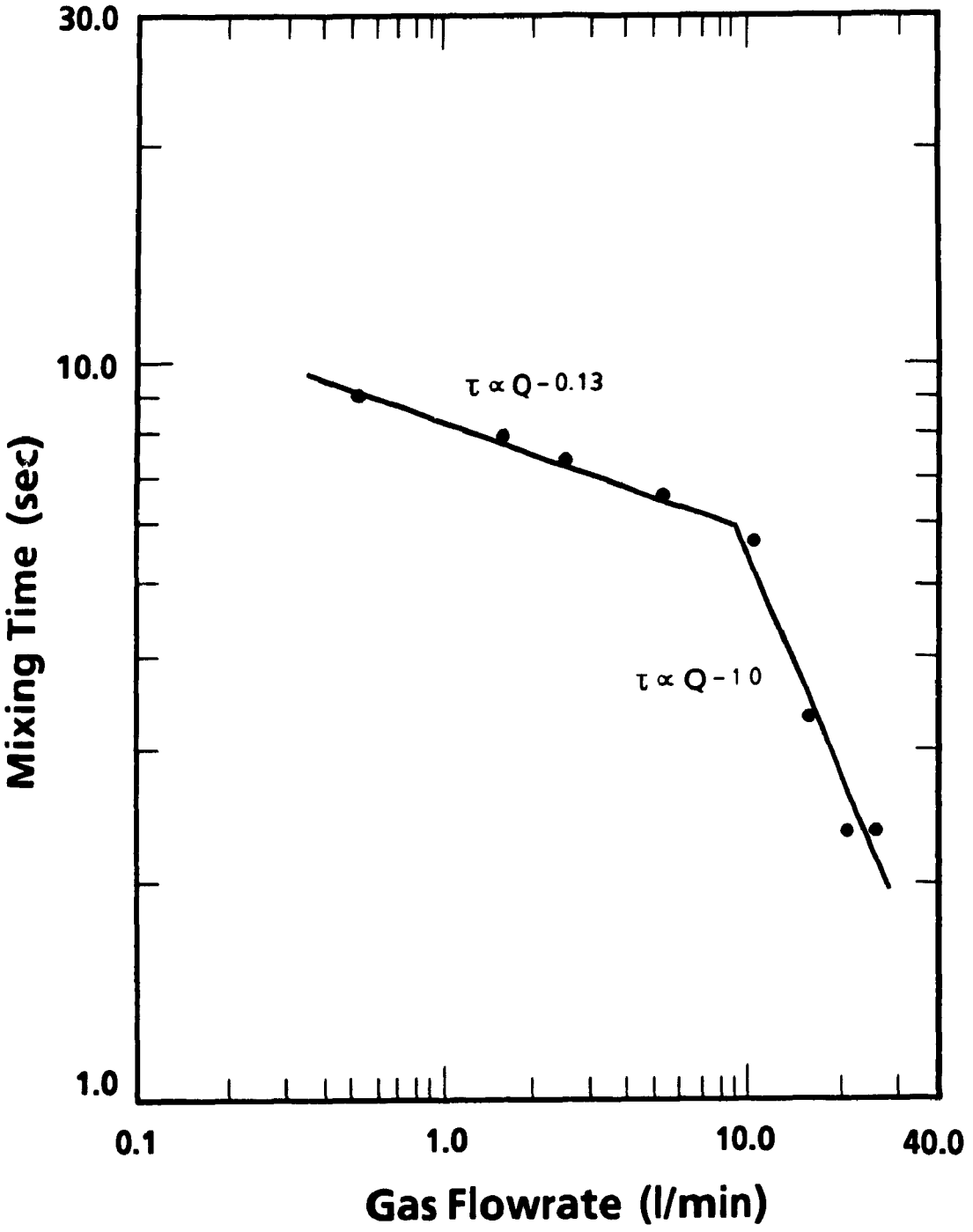

Figure 3.4 Mixing Time Behaviour for a Bath Containing a Rigid Surface

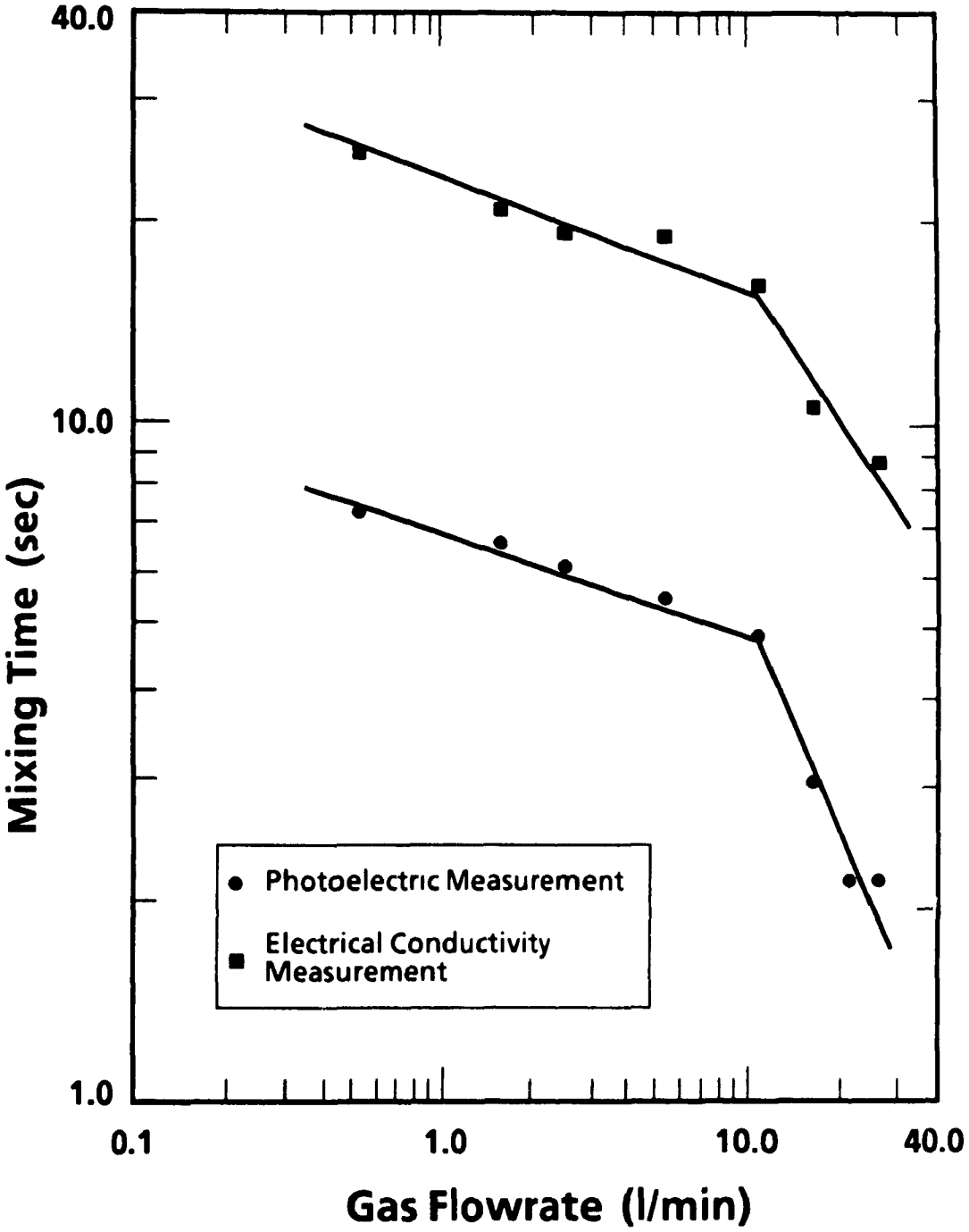

Figure 3.5 Comparison of Mixing Time Behaviour for a Bath Containing a Rigid Surface as Measured by Two Techniques

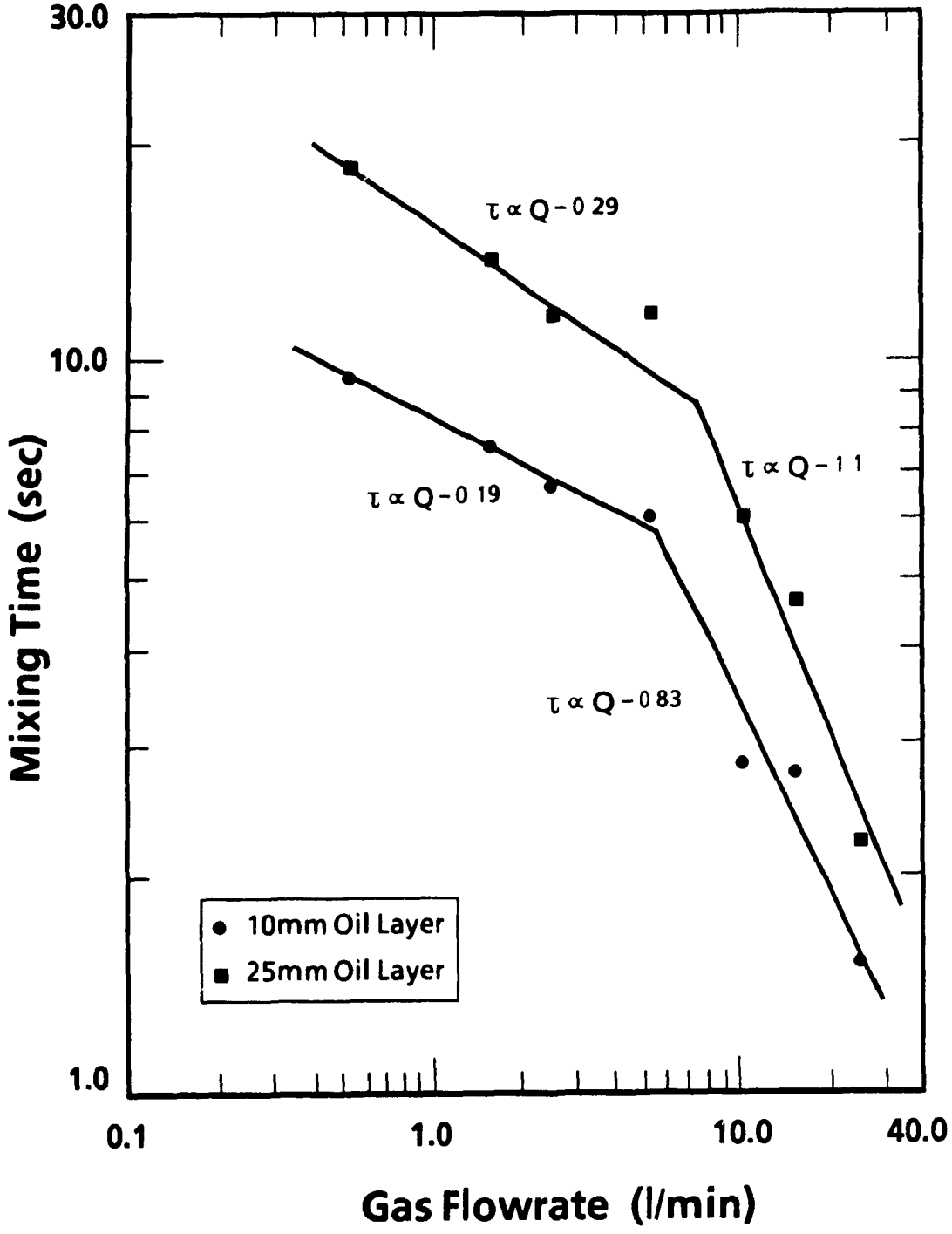

Figure 3.6 Mixing Time Behaviour for a Bath with an Oil Layer 10 and 25mm Thick

Table 3.1 Summary of Mixing Time Equation Exponents

Upper Surface Configuration	Flowrate Exponent	
	Low Q (<5l/min)	High Q (>10l/min)
Free Surface	-0.19	-0.19
1.0cm 20cs	-0.25	-0.76
50cs	-0.19	-0.83
1.6cm 20cs	-0 19	-0.51
50cs	-0.25	-1.3
2.5cm 20cs	-0.34	-0.97
50cs	-0.29	-1.1
1 0cm Wooden Surface	-0.13	-1.0

An experimental investigation of fluid mixing in gas stirred cylindrical vessels performed by Krishna Murthy et al. [48] showed somewhat similar changes in the value of n as those presented here. However, all tests performed by the authors contained gas injection into a single liquid. A thin upper layer was not included. For a bath depth equal to that used in this study the authors reported a change in the value of n from 0 138 to 0.438, with the shift being associated with the onset of plume swirling. This is in contrast to the observation made in this study in which the mixing time curve remained linear over the entire range of gas flowrates selected when only one liquid was being stirred. The onset of plume rotation did not appear to cause a change in the mixing behaviour of the bath. Instead, the shift in the mixing time curve occurred in the presence of a second phase on the surface of the bath. Under these conditions, as noted earlier, plume rotation did not occur in the range of gas flowrates tested.

From the flow visualization experiments, it was found that in the case of the oil-free system no significant qualitative difference was found in the flow pattern of the water over the entire range of gas flowrates employed. The pattern remained as a single recirculatory loop encompassing the whole field

of view. Therefore, the mixing time would be expected to decrease monotonically as the speed of recirculation increased. This is borne out by the straight line relationship shown in Figure 2.2.

For the oil covered systems, the photographs of the fluid flow field indicate that beyond a threshold flowrate, changes in both the level of turbulence, as indicated by an increase in the chaotic nature of the fluid flow patterns, and the shape and number of recirculation loops, occurred. For relatively thin oil layers, the flow pattern is comprised of a single convection loop, but after a flowrate of 5-10l/min, the level of turbulence seemed to be significantly increased. Therefore, at high flowrates the diffusive component of the mixing is increased and the mixing time decreases at a rate greater than that for a strictly recirculating flow.

In the presence of a thicker oil layer multiple convection loops were generated and the diffusion of material across the boundary between the zones led to slow homogenization. When the gas flowrate was high enough to impart sufficient energy to break up the oil layer, the multiple zone configuration was replaced by a larger main zone incorporating the plume region and a smaller zone near the wall close to the oil/water interface. Associated with this redirection of flow was an increase in turbulence. Therefore, mixing at higher flowrates would be expected to be much faster, leading to the sudden transition in mixing behaviour, as shown in Figure 3.6.

The variation of mixing time with gas flowrate is expected to incur another change as the flowrate is increased beyond the range stipulated for this study. For extremely high volumes, the injected gas would begin to channel through the bath producing a plume of lower volume fraction of water. Kato et al.[49] have derived an empirical relationship for the "blow-by" gas flowrate as a function of bath depth and tuyere diameter. The authors reasoned that for a gas jet, or plume, to remain continuous at all points in the bath the dynamic pressure of the jet must be greater than the static pressure of the bath at any location, assuming no reactions occur between the gas and the surrounding fluid. If a continuous jet passes through the bath the conditions for blow-by to occur will have been attained. The pressure balance is given by equation 3.1

$$\frac{1}{2}\rho_g u^2 > \rho_l g\,(H-y) \tag{3.1}$$

where u is the gas velocity at the vertical position y, in a bath of depth H. The empirical model used by the authors to describe the gas velocity in a rising plume is given by equations 3.2 a and b.

$$u = U\,(y_O / y) \tag{3.2a}$$

$$y_O = 6.2\,d \tag{3.2b}$$

where U is the gas velocity at the tuyere tip and d is the tuyere diameter. Combining these equations gives the following:

$$z(y) = \rho_l g y^3 - \rho_l g H y^2 + \frac{1}{2}\rho_g U^2 (6.2d)^2 > 0 \tag{3.3}$$

For the equation z(y) = 0 to have only one negative real root, the authors determined that:

$$H < 1.5\left(\frac{\rho_g U^2 (6.2d)^2}{\rho_l g}\right)^{1/3} \tag{3.4}$$

Therefore, the critical bath height,H, for a given flowrate, Q injected through a tuyere of diameter d, is given by equation 3.5, where all quantities are given in appropriate SI units.

$$H = 2.778\left(\frac{\rho_g Q^2}{\rho_l d^2}\right)^{1/3} \tag{3.5}$$

Using this formula, for a bath depth of 125mm, including a thick oil layer, the blow-by gas flowrate for the present model would be $3.99 \times 10^{-4} m^3/s$

(24l/min), which was at the upper end of the range of flowrates used. Therefore, gas blow-by would be expected to be present at flowrates slightly higher than those used

The reduced volume fraction of water in the plume would result in a possible reduction, or stablization, of the convective component of mass transport, which may or may not be off-set by an increase in the level of turbulence in the bath. Also, the additional gas would simply by-pass the system and its energy input would not be imparted to the fluid Therefore, it is believed that any further increase in gas flowrate would not produce a significant decrease in the mixing time and a lower limit of this variable would be expected.

3.1.3 Mixing Time Versus Slag Thickness

The previous analysis has considered the influence of the gas flowrate on the trend of mixing time. Figure 3.7 shows the effect of the thickness of the upper layer on the mixing time for various gas flowrates. Again, the mixing behaviour can be divided into two groups with 5l/min being the transition flowrate. For low gas flowrates, the mixing time did not change significantly as the oil layer thickness was increased to 7mm Beyond this value the mixing time increased rapidly. Mazumdar, Nakajima and Guthrie[29] showed that the presence of a second immiscible liquid increases the time for homogenization by reducing the fraction of input energy available for the generation of fluid flow. The consumption of energy was concluded to be a result, mostly, of potential energy losses associated with the distortion of the oil/water interface and, to a lesser degree, from energy losses associated with oil droplet formation and entrainment. However, in this low range of gas flow there was no appreciable increase in the interface distortion as the thickness of the oil layer was increased. The sharp increase in mixing time shown in Figure 3.7 was a result, rather, of a change in the bulk flow pattern. Thus, a thicker upper layer, and an energy input insufficient to break up the layer, results in the formation of multiple recirculatory zones, as shown in figures 3.1d and 3.2. The transport of an added tracer across the boundary

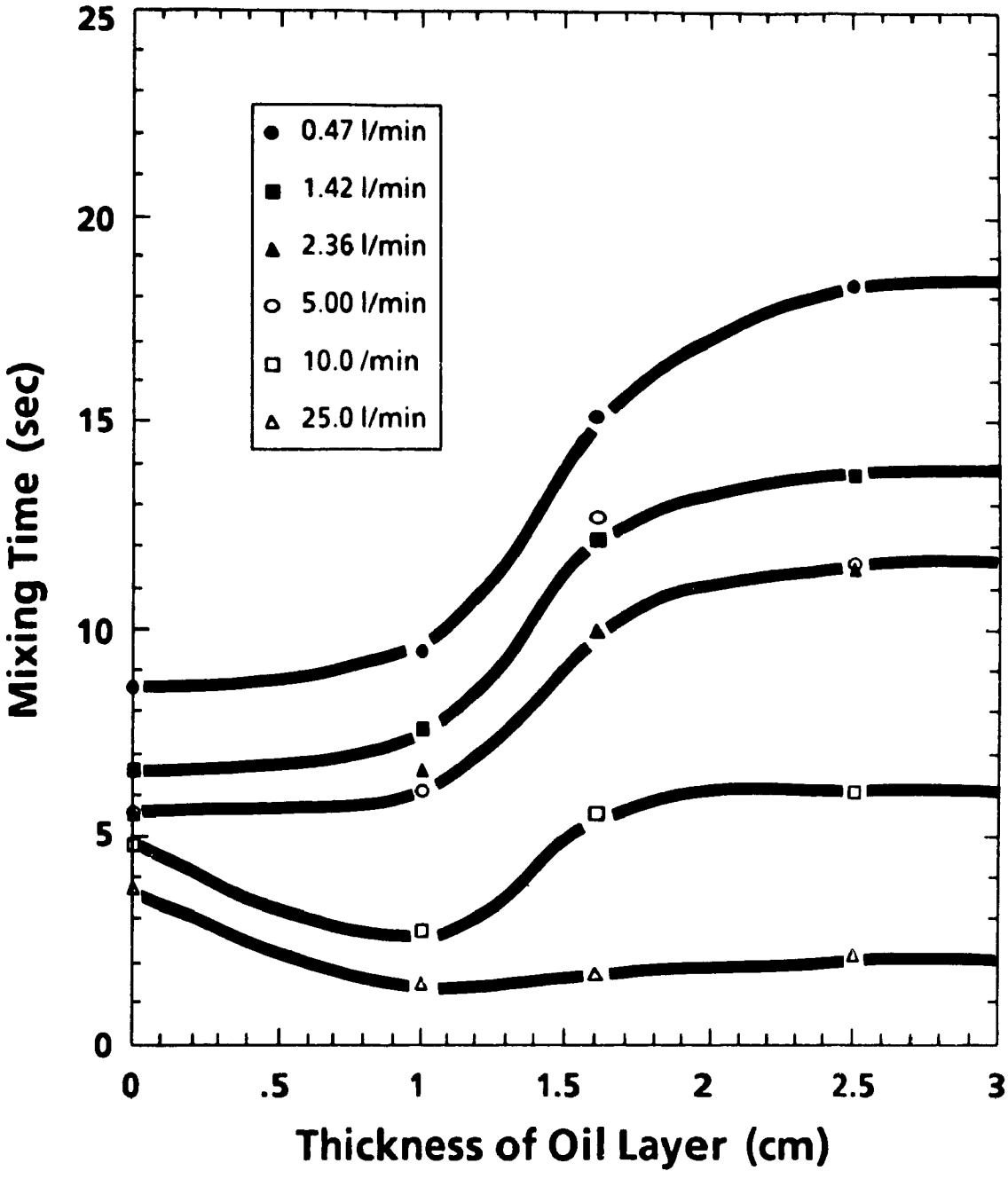

Figure 3.7 Variation of Mixing Time with Depth Oil Layer

between the zones is accomplished by diffusion, which is a slow process. Therefore, the multiple zone configuration causes slower mixing. The increase in mixing time then reaches an upper limit as the layer thickness increases further past approximately 20mm, depending on the gas flowrate Any further increase in the thickness does not create any more change in the general flow pattern of the tight recirculatory loop near the plume.

The second flowrate range, i.e. >5l/min, is relatively insensitive to slag thickness. The energy input appears to be high enough to break up the slag layer and prevent the formation of multiple recirculatory zones Also, the increase in mixing time as a result of energy consumption through oil entrainment and interface distortion seems to be offset by the sharp decrease in mixing time through enhanced turbulence, as discussed previously. At extremely high flowrates, this off-setting characteristic even results in mixing times lower than that measured for the free surface configuration. The increase in turbulence also enhances diffusion even if multiple zones are created, thereby reducing the effect of such zones

The influence of slag thickness on the mixing behaviour is most significant in gently stirred vessels which contain a significant layer of slag. In such configurations the vertical redirection of fluid pumped by the two-phase plume is more prevalent than if either the layer were thinner or the energy level of the slag/metal interface was high enough to cause a loss of slag layer integrity. This was also noted by Matway[50] who remarked that the presence of a thick oil layer produced a turbulent zone near the plume and a relatively calm bath outside of this zone.

To the extent that the energy level at the interface is important, it would seem logical that the depth of the bulk fluid would be another variable to be considered when studying the redirective capability of a slag layer. The system studied had a rather shallow bath, having an aspect ratio of 0.33 For a deeper bath a greater volume of fluid would be entrained into the plume, thereby increasing the momentum of the plume. However, this would be counter-balanced by the dissipation of energy as the plume rose through the bath. The effects of bath depth on mixing, for a given thickness

of the upper layer, would have to be studied using mixing time measurements and flow visualization experiments.

3.1.4 Effect of Oil Viscosity

The viscosity of the upper layer had an affect on the mixing time, but only at a thickness greater than 10mm, and only at low gas flowrates As is shown in Figure 3.8, a less viscous oil produced slightly longer mixing times A close study of the interaction of the plume and the upper layer by Matway showed that lower viscosity oils tended to produce smaller plume-eyes Therefore, the tight recirculatory loop generated near the plume will be smaller for such systems and hence slower recirculation and mixing in the remainder of the bath. This is displayed by the longer mixing times for the system containing the lower viscosity oil.

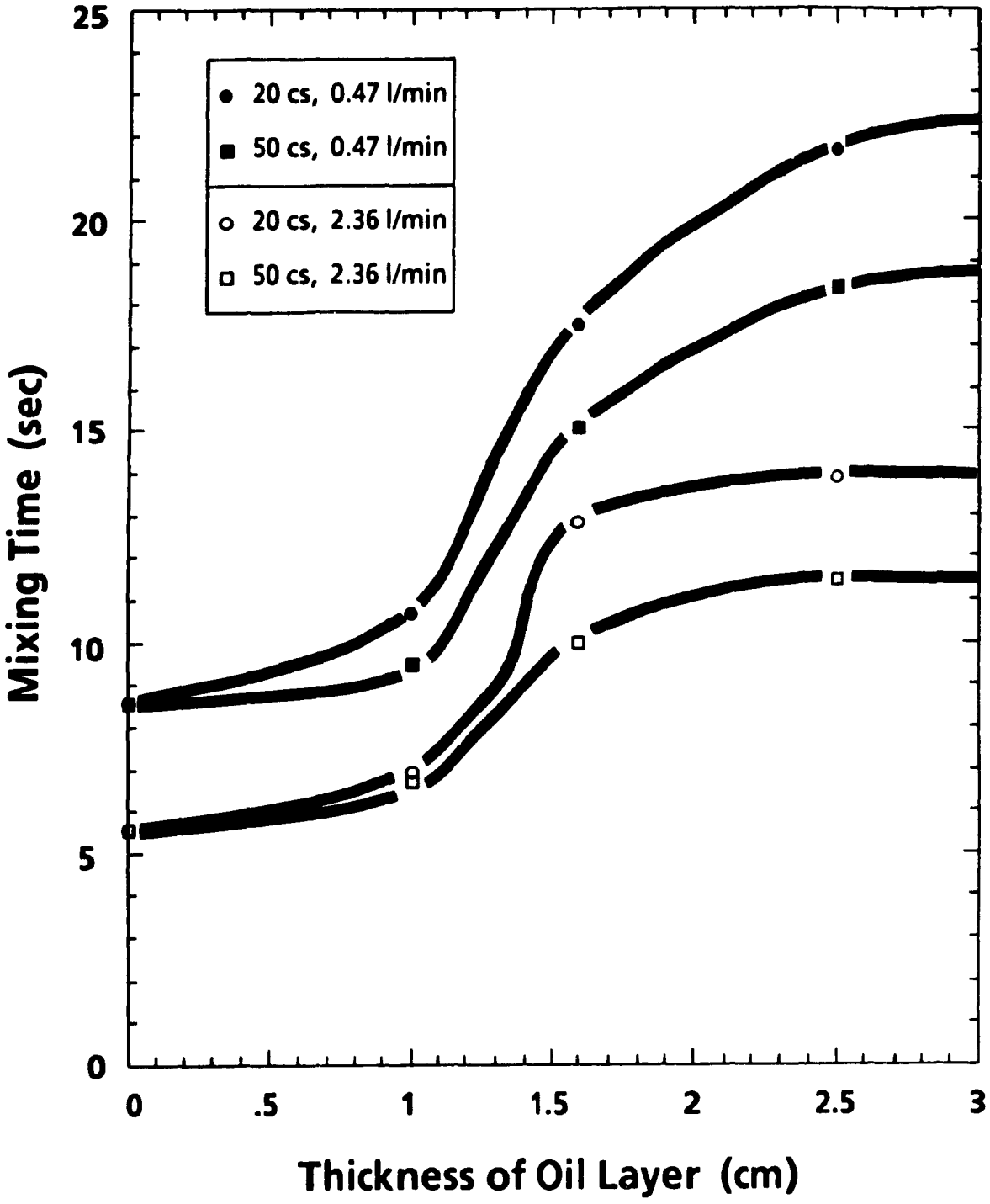

Figure 3.8 Variation of Mixing Time with Thickness and Viscosity of Upper Layer

3.2 Entrainment Behaviour

The entrainment behaviour of the gas stirred system was monitored at nine locations in the bath and was characterized by the number of entrained oil droplets and air bubbles per unit volume of fluid as a function of the gas flowrate and thickness of the overlying layer. Only one viscosity of oil was used in this section of the study.

3.2.1 Behaviour of the Upper Layer and Droplet Size

It was found that the nature of the oil layer was dependent on the gas flowrate and the length of time that stirring was maintained. At low flowrates, the integrity of the layer was not altered, except that the oil in the central region was displaced by the two-phase plume. This displacement exposed the water to the air. The interface between the remaining layer and the water was quiescent, as was the free surface of the oil, with low amplitude ripples adjacent to the plume. This configuration remained constant over extended stirring times. At slightly higher flowrates, around 5l/min, a portion of the oil layer began to break up into large droplets, approximately 10-20mm in diameter, and migrate towards the wall of the vessel. The large oil droplets remained very close to the liquid/liquid interface as the fluid velocity was insufficient to entrain them to any significant depth.

Tanaka used the concept of the Helmholtz stability criterion to estimate the maximum stable droplet diameter produced by the shearing action at the interface between the two liquids.[33] The author presented the following equation relating the droplet size to a critical Weber number for the system.

$$(N_{We})_{crit} = \frac{\rho_{l1} \bar{v}^2 d_{max}}{\sigma} \qquad (3\ 6)$$

where

$$\bar{v}^2 = 2.0\left(\frac{\varepsilon\, d_{max}}{\rho_{l1}}\right)^{2/3} \tag{3.7}$$

The author also presented a value of 1.2 for the critical Weber number. The term ε is the input energy, in units of $Wm^{-3}s^{-1}$. The energy is supplied by the injected gas and is comprised of two components; buoyancy and kinetic energy. For the system under study, these equations can be rearranged to give the following equation relating the droplet size, with the units of meters, explicitly as a function of the energy input.

$$d_{max} = 0.0898\,\varepsilon^{-0.40} \tag{3.8}$$

At low flowrates the buoyancy energy is dominant while the kinetic energy is dominant at high flowrates, if no energy is lost during the initial expansion of the plume as the air enters the bath. These energy terms are calculated using equations 3.9 and 3.10, respectively.

$$\varepsilon_{bouyancy} = \frac{371\,Q\,T}{V}\,ln\left(1.0 + \frac{9.8\,\rho_{l1}\,L}{P_0}\right) \tag{3.9}$$

$$\varepsilon_{kinetic} = \frac{1}{2}\,\frac{\rho_g}{V}\,\frac{Q^3}{A^2} \tag{3.10}$$

The Stoke's rising velocity equation can be used to estimate the size of droplets which would be maintained in the lower phase due to the fluid motion. The maximum diameter of a droplet is expressed by equation 3.11

$$d_{max} = 2\left(\frac{9}{2g}\,\frac{\mu_{l1}}{(\rho_{l1}-\rho_{l2})}\,U\right)^{1/2} \tag{3.11}$$

where U is taken as the mean speed of recirculation of the bath. To estimate the mean speed of recirculation, the equations developed by Sahai and Guthrie to calculate the mean plume velocity with a correlation to the mean fluid speed, were used.[13,51]

$$U_p = 4.19\left(\frac{L^{1/4}Q^{1/3}}{R^{1/3}}\right) \tag{3.12}$$

$$U = 0\,18\,\frac{U_p}{R^{1/3}} \tag{3.13}$$

Combining the equations yields

$$U = 0\,754\,\frac{L^{1/4}Q^{1/3}}{R^{2/3}} \tag{3.14}$$

where the dimensional constants are expressed in SI units.

Studies of gas stirred ladles by Krishna Murthy et al.[52], and Haida and Brimacombe[53] showed that only a fraction of the kinetic energy of the input gas stream is transmitted to the bath, with estimates of 20 percent being suggested. Therefore if only the bouyancy energy is considered, by replacing the quantity Q by the energy input, using equation 3.9, the maximum droplet diameter in the model system can be expressed by equation 3 15 for the bouyant energy dominated range.

$$d_{max} = 1\,153\times 10^{-3} * \varepsilon^{1/6} \tag{3.15}$$

The dimensional constants in equations 3.8 and 3.15 were calculated by substituting the values for the model system into the equations from which they were derived. All quantities used in the calculations, and the variables in the equations, were in the appropriate SI units.

If equations 3.8 and 3.15 are plotted together, as shown in Figure 3.9, it is possible to compare the stable size of droplets produced and the maximum

droplet diameter which can be entrained. All droplets in the region below the Stoke's rising velocity line will be entrained in all regions of the bath. The droplets in the region below the Helmholz stability line will be readily generated. Therefore, the double shaded region represents the size of droplets, below the maximum stable size, which will be entrained into the bath. The larger droplets in the single shaded region above this section will only be entrained into zones of high velocity downwards fluid motion, such as near the interface of the two liquids. The other significant zone is the single shaded region situated to the right of the intersection of the two lines. This region represents the energy levels in which all of the droplets generated will be entrained into the entire bath volume

At a low flowrate of 0.47l/min, the energy input is of the order of 1.0 kg m^{-3} sec^{-1} while at a flowrate of 5l/min, the energy is around 25kg m^{-3} sec^{-1}. For these flowrates, the estimated maximum stable droplet would be 90mm and 25mm, respectively. The value of 25mm corresponds well to the visual estimations of the size of the large droplets seen in the model at a flowrate of 5l/min. As blowing continued at this rate, the size of the droplets was reduced to a constant size of approximately 5mm after 15 minutes of operation All dimensions were approximated by visual examination of the model during the course of the experiments. For the upper end of the flowrates tested, an estimate of 4mm is predicted by the Helmholtz's stability criterion, which also corresponds well to visual observations of entrained droplets.

At very high flowrates, the disintegration of the oil layer was very rapid and the size of the droplets was constant with time at approximately 3-5mm in diameter. Similar observations were made by Lui, Kaiwen and Ting[54] during experiments involving mass transfer between two liquids phases in gas stirred reactors. The lose of integrety of the oil layer was accompanied by an increase in the thickness of the overlying layer. As the layer broke down an emulsion, in kind, was formed with the water thereby increasing the thickness of the layer. At higher gas flowrates, the emulsion was further thickened by the downward motion of the bulk fluid.

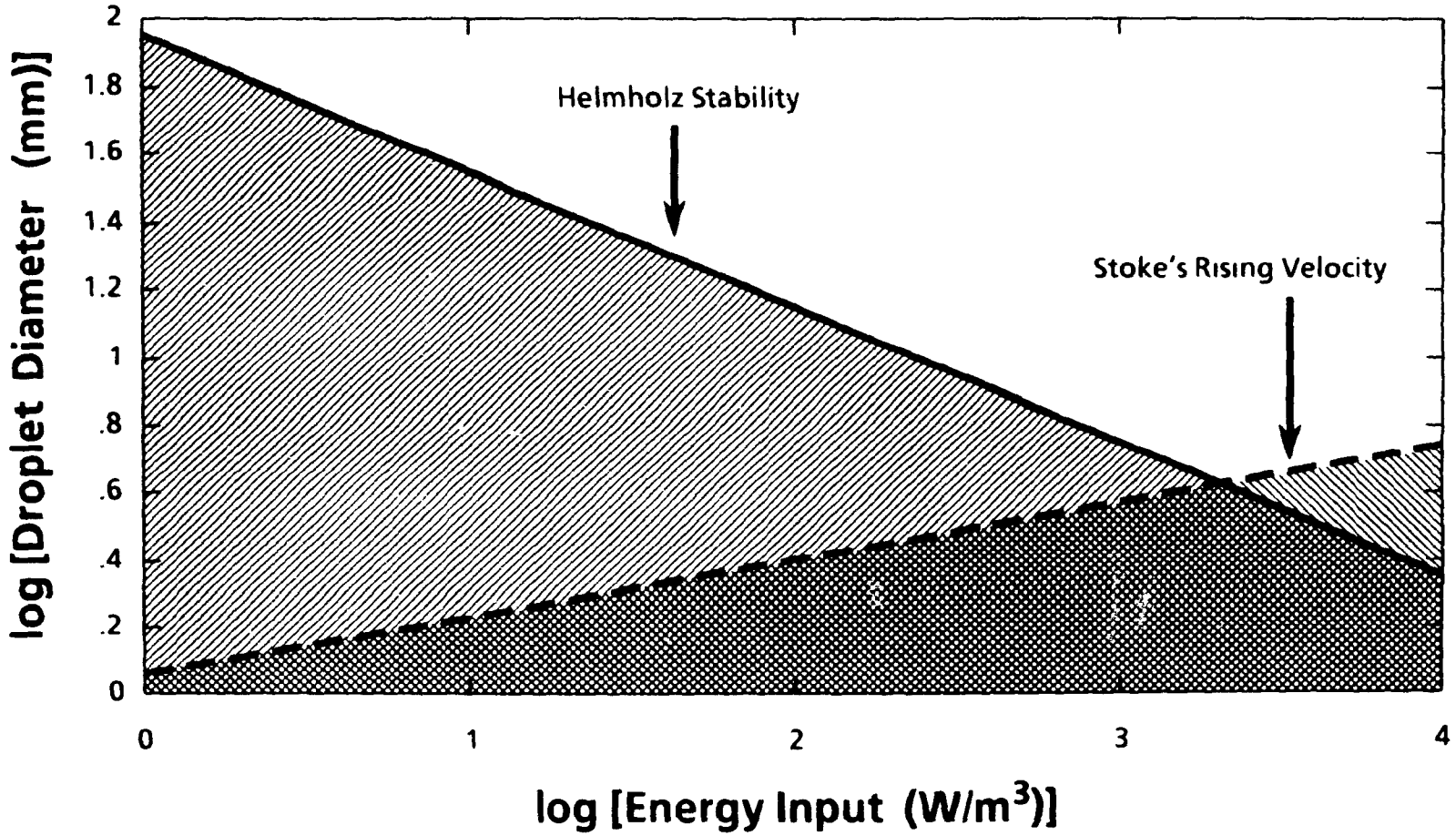

Figure 3.9 Comparison of the Size of Stable Droplets Generated and the Size of Entrained Droplets for Model

Using the procedure outlined in the Appendix of this study to calculate the size of the droplets as measured by the electronic sensor, it was found that a large number of smaller droplets were detected throughout the vessel at all gas flowrates. An attempt at estimating a droplet size distribution was made. The majority of the sensor readings were approximately 10msec in length, indicating a droplet diameter of roughly 2.5mm. A range of sensor responses from 3 to 50msec was measured. This translates into a range of droplet diameters from 1.5 to 5.0mm

3.2.2 Entrainment versus Gas Flowrate

In order to analyze the effect of the gas flowrate on the entrainment of oil droplets, one sampling location, situated at midradius near the bottom of the vessel, was used Two thicknesses of oil were considered for tests at flowrates of 5, 10, 15 and 25l/min. Figures 3 10 and 3 11 show the concentration of oil droplets, specified by the number of droplets counted via the photoelectric sensor per litre of fluid drawn from the sampling location, as a function of time after the initiation of gas injection for a system containing a 10mm thickness of oil. For the lower flowrates, a constant degree of entrainment was measured almost immediately after the start of gas injection. The values are approximately 325 droplets/litre at a blowing rate of 5l/min and 700 droplets/litre at 10l/min.

As is seen in Figure 3.11, beyond a flowrate of 10l/min, the concentration of entrained droplets increased dramatically with the continuation of blowing. This rapid increase then stops with the concentration, or number density of droplets, levelling out at approximately 17500 droplets/litre. This extremely high concentration of droplets near the bottom of the vessel could only be possible if the droplets were small enough to resist the buoyancy and convective forces of the circulating water. From the discussion of the mixing behaviour, it was noted that at high flowrates, the level of turbulence in the bulk liquid increased greatly. This increase in energy would also appear to be responsible for the continual break-up of larger entrained droplets into smaller ones. The disintregration of droplets would eventually be offset by the coagulation of small droplets when the concentration became too great. Therefore, as was measured, a new

equilibrium level of droplet concentration was attained when the energy level of the bath is very high.

Similar results were obtained for a thicker oil a layer. Figures 3 12 and 3.13 show the concentration versus time measurements for a 25mm oil layer at the same gas flowrates. By comparing these figures to the previous two, it can be seen that the droplet concentration levels at the lower flowrates are slightly higher for the thicker oil layer. The increase in dropet entrainment with the thickness of the overlying layer was also noted by Tanaka. This is possibly due, in part, to the increased volume of oil displaced from the eye of the plume during gas injection. Another interesting feature to note is that the flowrate at which the concentration shifts from constant to rapidly increasing is greater for the thicker oil layer It appears, however, that the upper level of the droplet concentration attained is roughly the same regardless of the thickness of the upper layer

3.2.3 Distribution of Entrained Phases

Presented in Figures 3 14 to 3.17 are entrainment distribution profiles of air and oil in the water for systems containing 10 and 25mm oil layers subjected to gas flows of 1.42 and 5l/min. These flowrates were chosen since, as was seen in the previous section, the entrainment behaviour is constant with time at flowrates below 10l/min. Monitoring was carried out at nine locations in one half of a vertical cross section of the vessel, as indicated in the figures. Droplet counts were carried out over a sampling time of 300 sec , with 8 tests performed at each location

At the low flowrate, the distribution of entrained oil is closely linked to the flow pattern of the bulk fluid. As was discussed in section 3.1 1, a thicker upper layer results in a system of multiple recirculatory zones with the strongest and narrowest zone located near the plume. By comparing Figures 3.14 and 3.15, it is seen that the concentration of oil droplets is lower in the majority of the bath for a thick layer with sharp increases near the plume For a thin oil layer, the concentration of droplets is somewhat more evenly distributed in the upper region, as would be expected in a system containing a single recirculatory zone. The entrainment of air appears to follow the

same trend as the oil. The concentration of air bubbles under the thick oil layer is negligible since the velocity of the bulk fluid is too slow in the large second recirculation loop to maintain the entrainment of air. Somewhat surprising is the extremely low levels of air entrainment in the tight, higher velocity primary recirculating loop near the plume

When the gas flowrate is increase to 5l/min (Figures 3.16 and 3.17) the concentration profiles for the two oil thicknesses were similar, although the magnitude of entrainment was greater, especially near the oil/water interface, for the thicker layer. The flow behaviour of the bulk fluid is expected to have been similar at this flowrate, as was discussed in an earlier section.

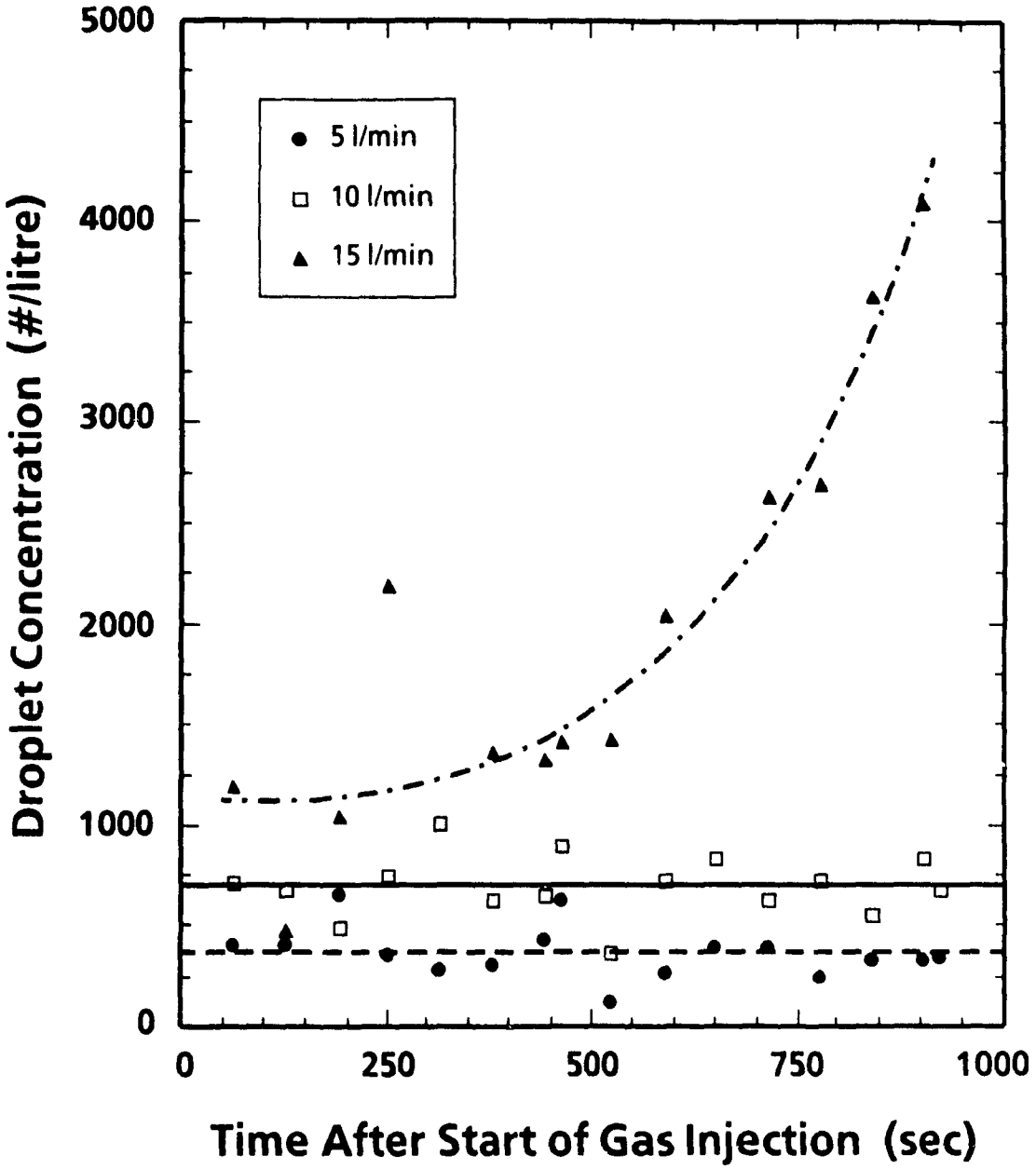

Figure 3.10 Concentration of Entrained Droplets, 1cm Oil: Gentle Agitation

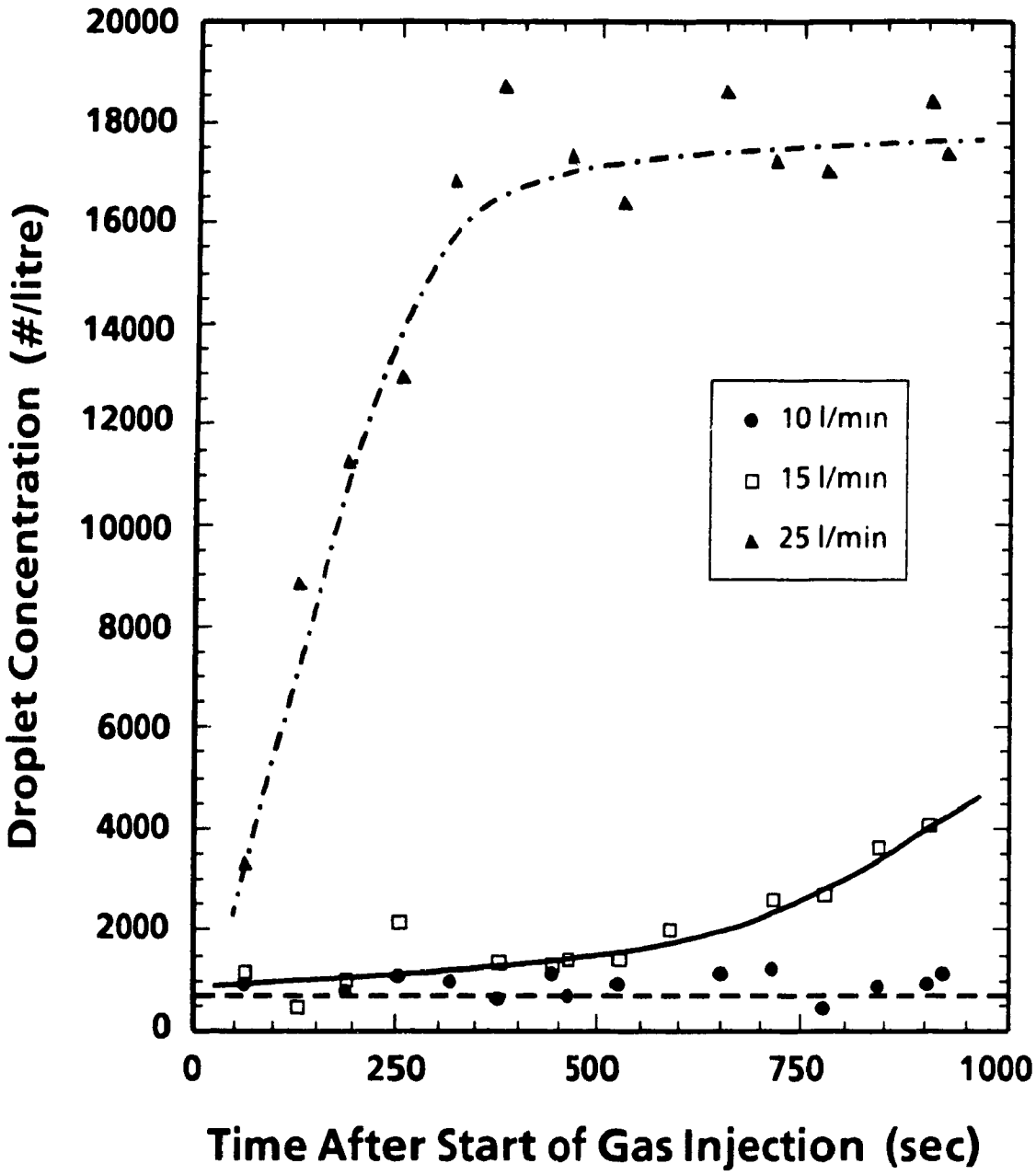

Figure 3.11 Concentration of Entrained Droplets, 1cm Oil: Intense Agitation

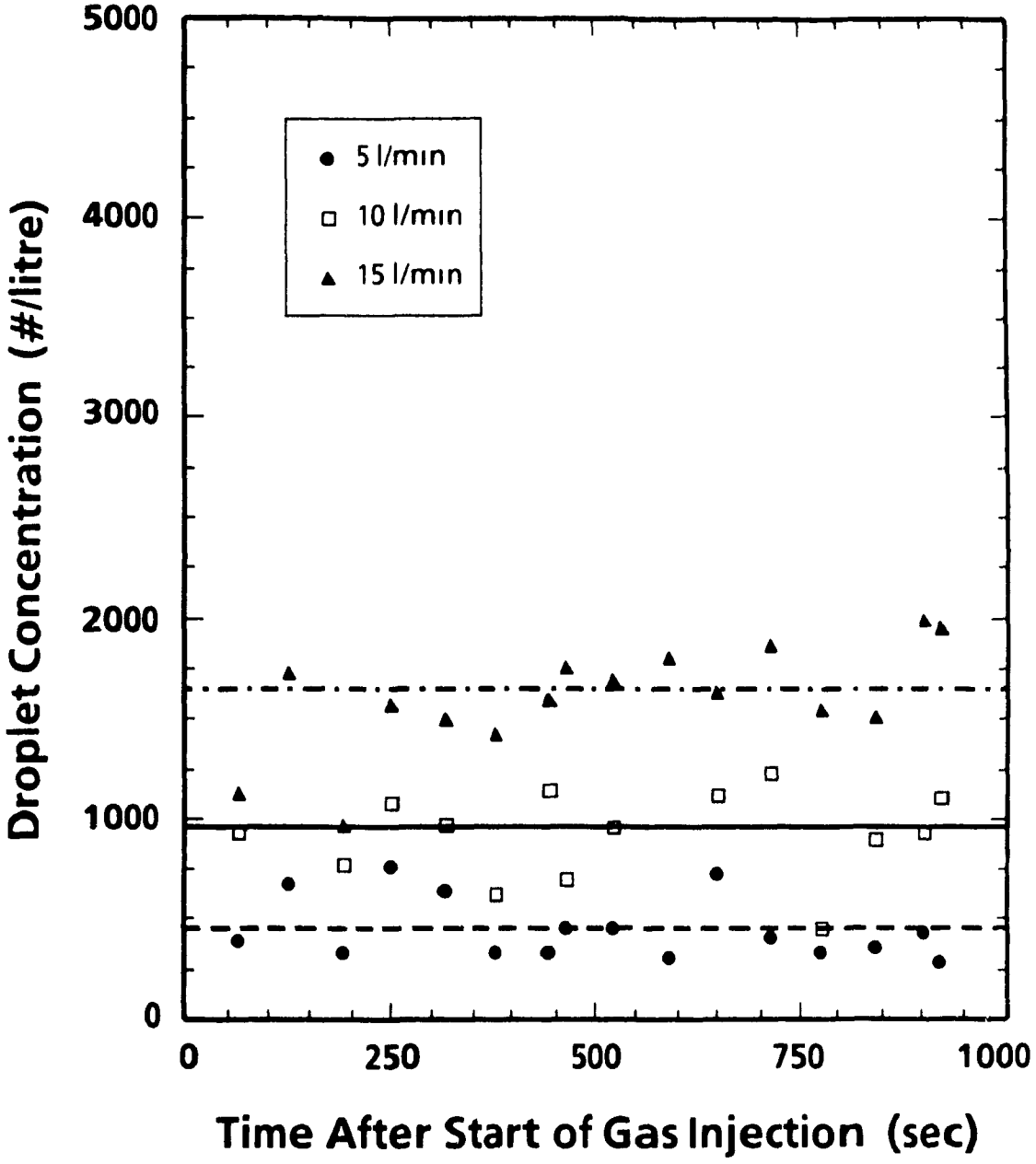

Figure 3.12 Concentration of Entrained Droplets, 2 5cm Oil: Gentle Agitation

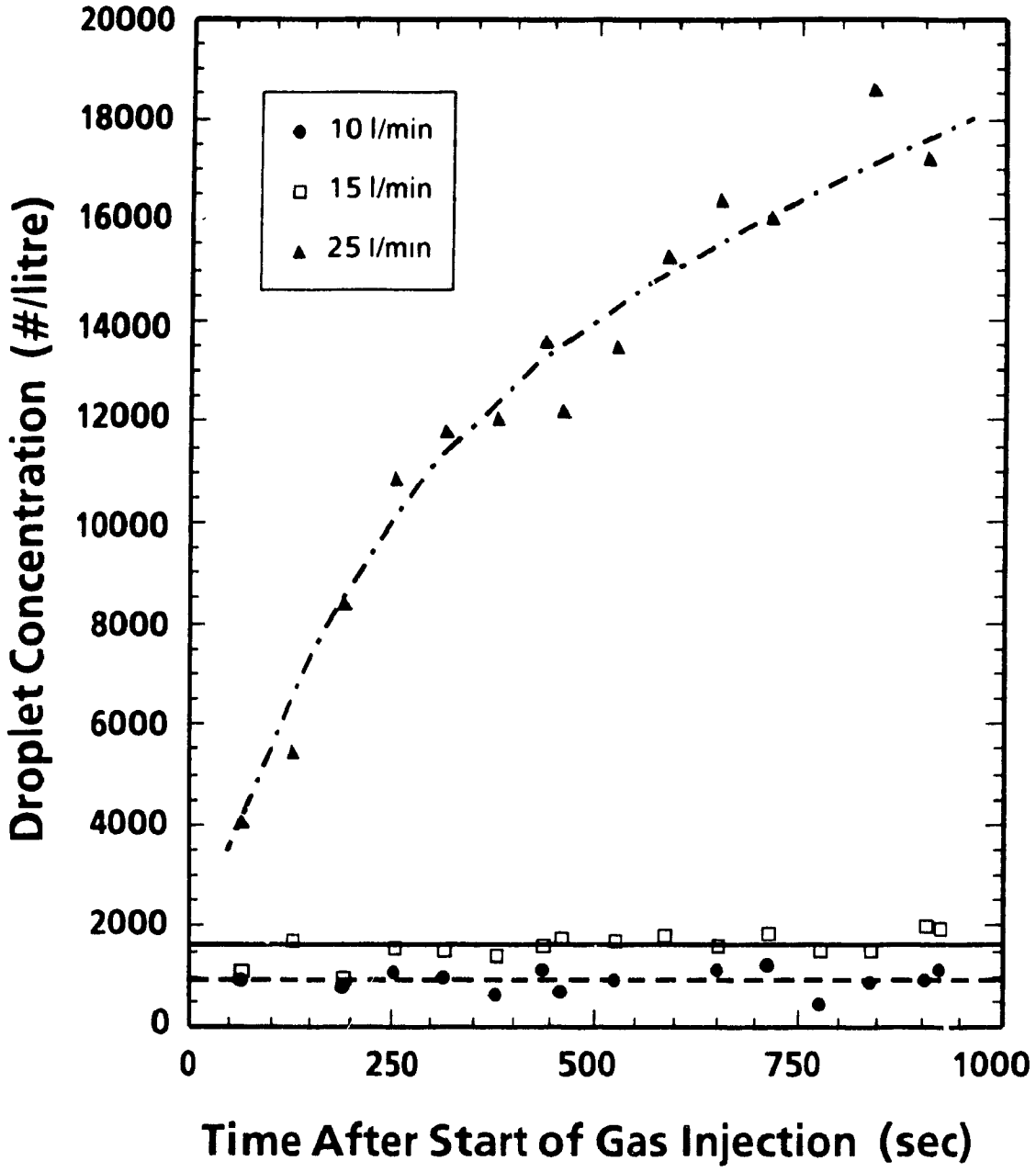

Figure 3.13 Concentration of Entrained Droplets, 2.5cm Oil: Intense Agitation

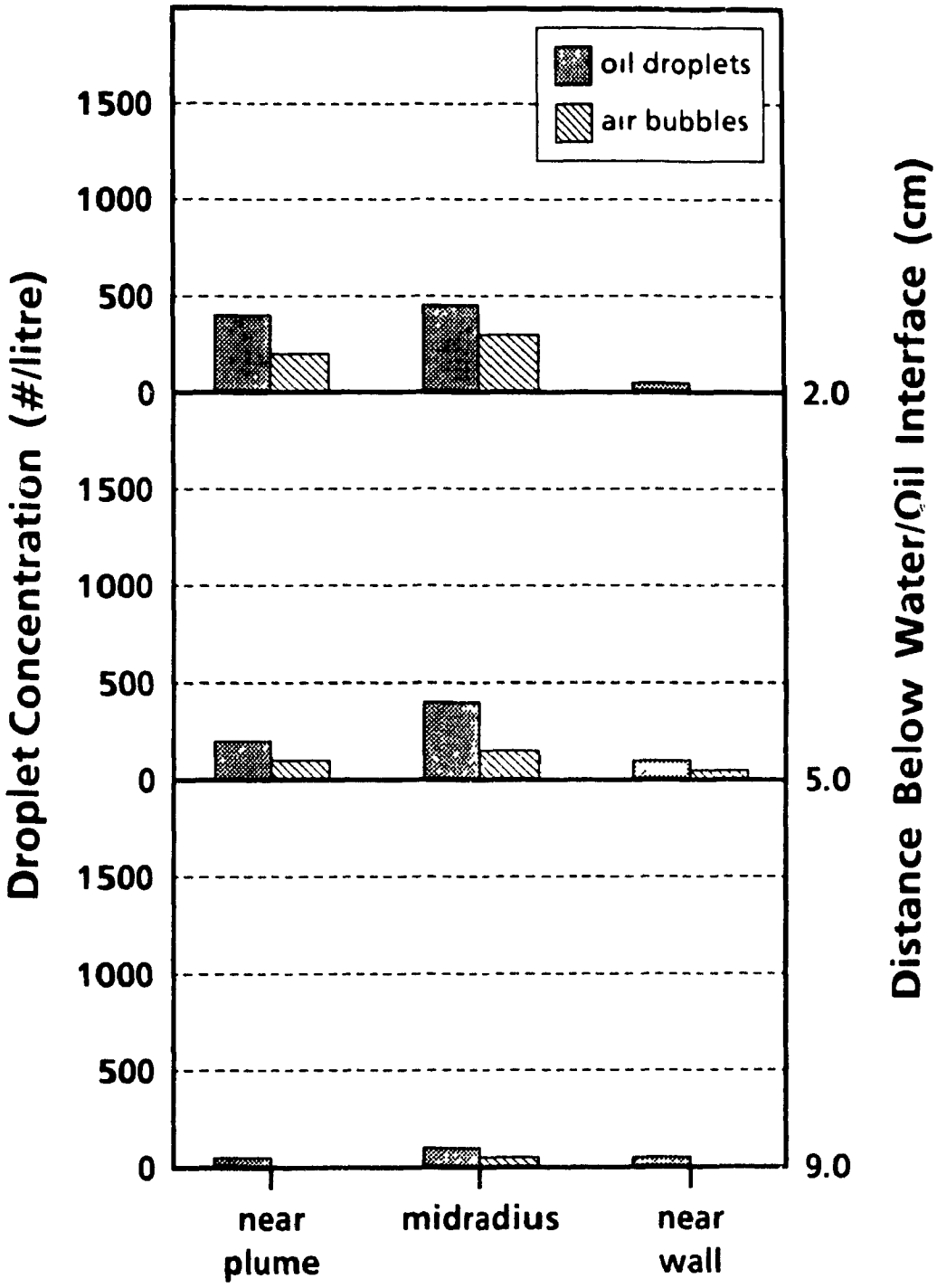

Figure 3.14 Distribution of Entrained Oil Droplets, 1 cm Oil and 1.42l/min Air

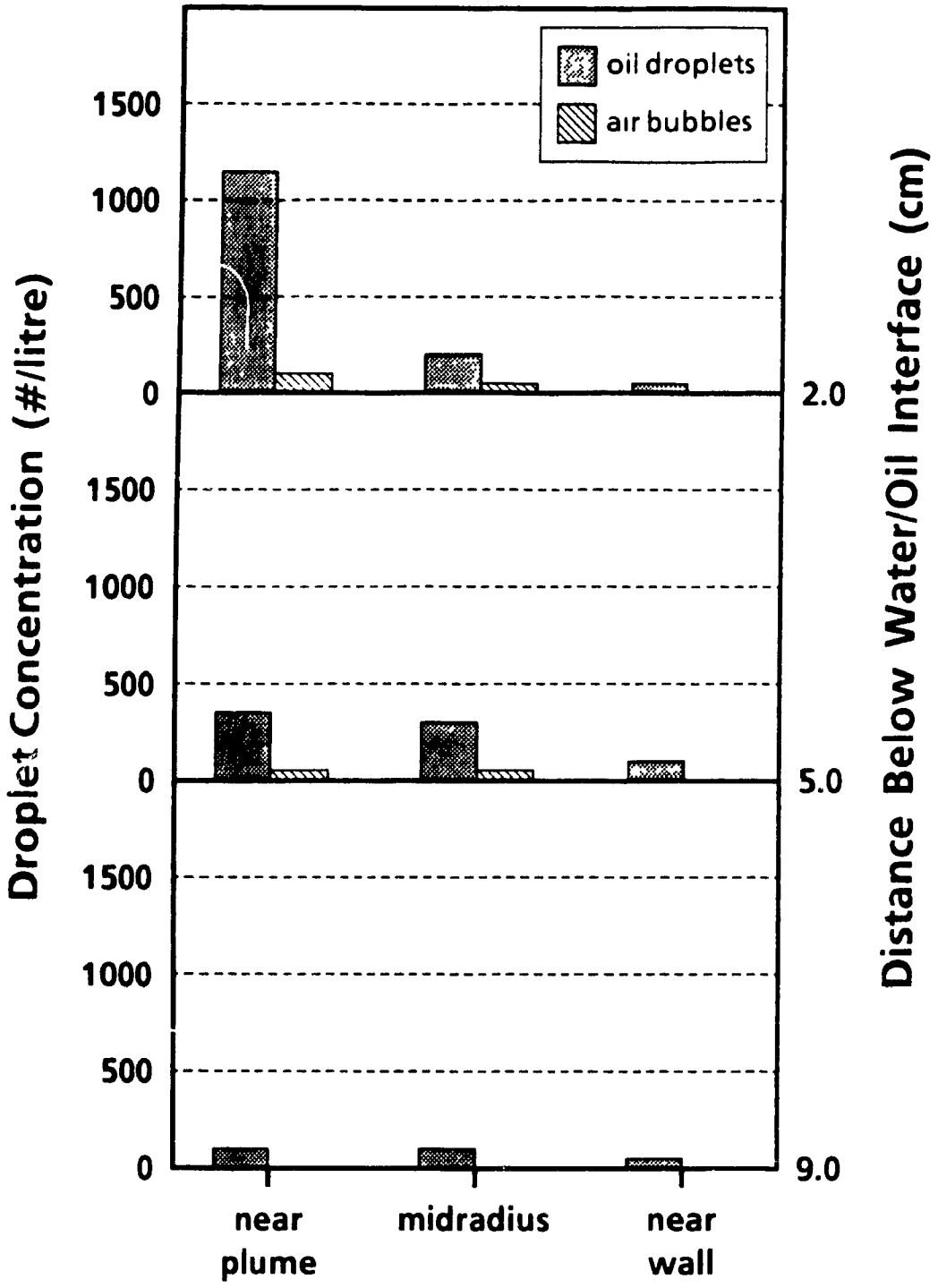

Figure 3.15 Distribution of Entrained Oil Droplets, 2.5 cm Oil and 1.42l/min

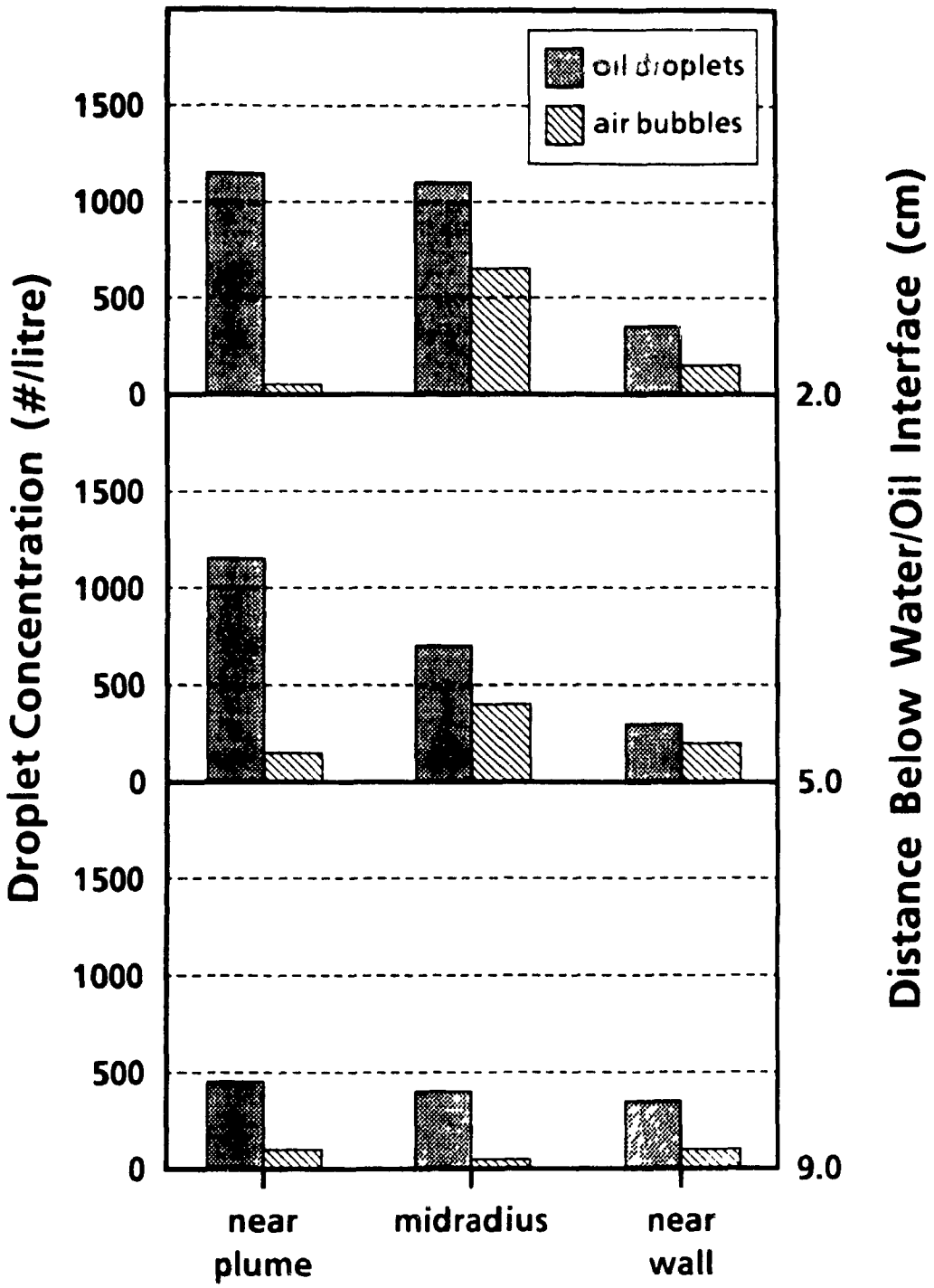

Figure 3.16 Distribution of Entrained Oil Droplets, 1 cm Oil and 5 l/min Air

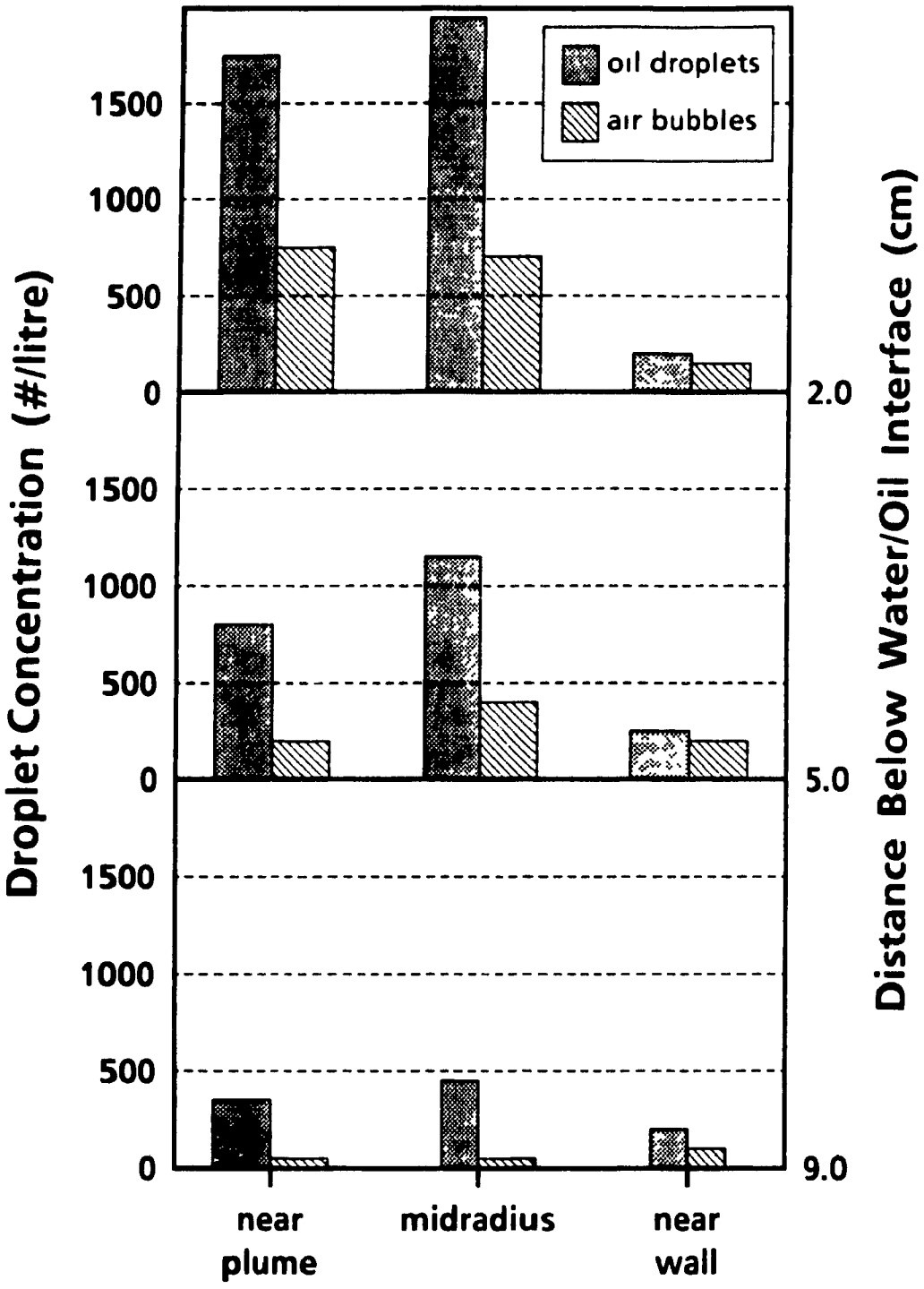

Figure 3.17 Distribution of Entrained Oil Droplets, 2.5 cm Oil and 5 l/min Air

3.3 Application to Industrial Operations

Since this study did not concentrate on the modelling of a particular process the results can only be applied in a qualitative manner Also, as was mentioned in Chapter 2, the interfacial surface tension between a slag and a metal phase may vary greatly during a treatment process. Therefore, the droplet size and number cannot be directly transferred to an industrial practice However, several important general conclusions can be drawn about the influence of a less dense liquid phase on the operation of a gas stirred vessel

The modified Froude number for various pyrometallurgical operations were calculated to compare with the range of values used in the study The processes are shown in Figure 3 18. Also indicated are the three zones of stirring intensities used in the model. gentle, intensive and a transition range. The transition zone corresponds to gas flowrates where the mixing time behaviour and the effect of the upper layer changed.

For gently stirred vessels, such as ladles used for refining operations, two strategies can be used if it is desirable to increase reaction kinetics between the bath and the slag The number of entrained slag particles can be increased by increasing either the thickness of the slag layer or the rate of gas input. Thicker slag layers generate more entrained droplets because the amount of material removed from the eye of the plume is greater, while greater gas flowrates provide more energy to create and entrain slag particles. However, thicker slags increase the mixing time of the bath while increased gas flowrates decrease the mixing time It was also noted that slags of higher viscosity aid in reducing the mixing time.

Systems falling within the intermediate range of Froude numbers are at the transition of mixing time and slag droplet entrainment behaviour For such operations a thinner slag will aid in increasing the degree of entainment for a given gas flowrate by reducing the flowrate require to attain the transition behaviour. A thinner slag will also ensure that the fastest mixing possible is achieved. Processes in this range may be at the level of energy input where the slag thickness has a strong influence on the mixing times

Therefore, it would be advisable that for thicker slags that as high an energy input as possible be used to ensure that the transition point is passed and the reaction kinetics maximized.

The good agreement between the size of the droplets seen in the model and the size predicted by the Helmholz stability criterion suggests that this criterion mcy be used to estimate the size of slag droplets which may be found in an industrial operation. Equations 3.8 and 3.15 were recalculated for a 150 ton argon-stirred steel refining ladle. The slag was assumed to have a density of 3000 kg/m3 and an interfacial surface tension with the molten steel of 1 10N/m The respective equations for the Stoke's and Helmholz formulae become:

$$d_{max} = 3\ 42 \times 10^{-4} * \varepsilon^{1/6} \qquad (3.16)$$

$$d_{max} = 0\ 133\, \varepsilon^{-0\ 40} \qquad (3\ 17)$$

These equations are plotted in Figure 3.19, together with the lines for the water/oil system for comparison The energy input to the steel, as a result of the injection of argon, is in the order of 10^3W/m^3. From the figure it can be estimated that there is sufficient energy to generate droplets of 6mm diameter. However, according to the terminal velocity equation only slag droplets of 1mm diameter would be found in the bulk of the bath. The larger droplets would only be found in regions of the bath where the fluid flow is greater than the average bulk veiocity

For a higher intensity vessel, such as the Q-BOP, where the energy input is in the range of 10^5W/m^3, the energy level is sufficient to break up slag droplets to a size of 1mm diameter. This is smaller than the size of particles which can be entrained, suggesting that these droplets would be dispersed thorughout the molten steel.

This analysis is consistant with the observations of the particles generated in the model. At low eneregy inputs larger particles were seen in the top regions of the bath with a few smaller droplets in the lower regions, while at high energy levels many very small particles were seen thorughout the bath.

One note to be made is that the Q-BOP operation may react differently than the model since the full scale operation involves more than one tuyere Therefore, the interaction of the various flow patterns may result in enhanced slag entrainment and more efficient mixing, which was not seen in the simple model

At the extreme case of gas stirring are the very intensively stirred operations. As small, high energy processes develop the mixing and entrainment characteristics studied will become important It was seen that the thickness of the slag layer does not significantly affect the mixing behaviour of the lower phase. This is valid only for the range of slag thicknesses modelled The results also indicate that very rapid reaction kinetics can be expected due to the entrainment of a large number of very small slag droplets

Finally, for all situations studied it was found that the presence of an upper liquid layer retards the generation of a swirling motion of the plume Therefore, it would seem apparent that the slag in the vessels of an industrial operations would help to maintain a steady plume.

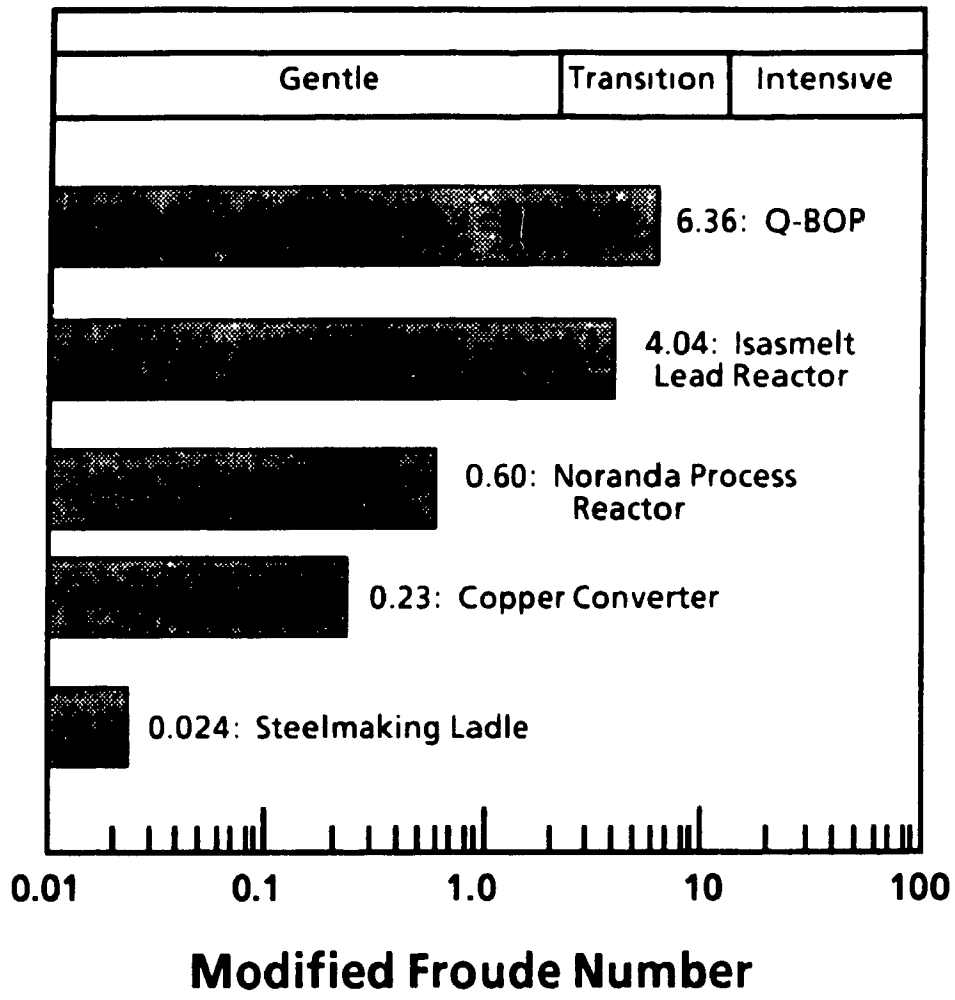

Figure 3.18 Comparison of the Modified Froude number for Various Industrial Operations to the Modelling Conditions

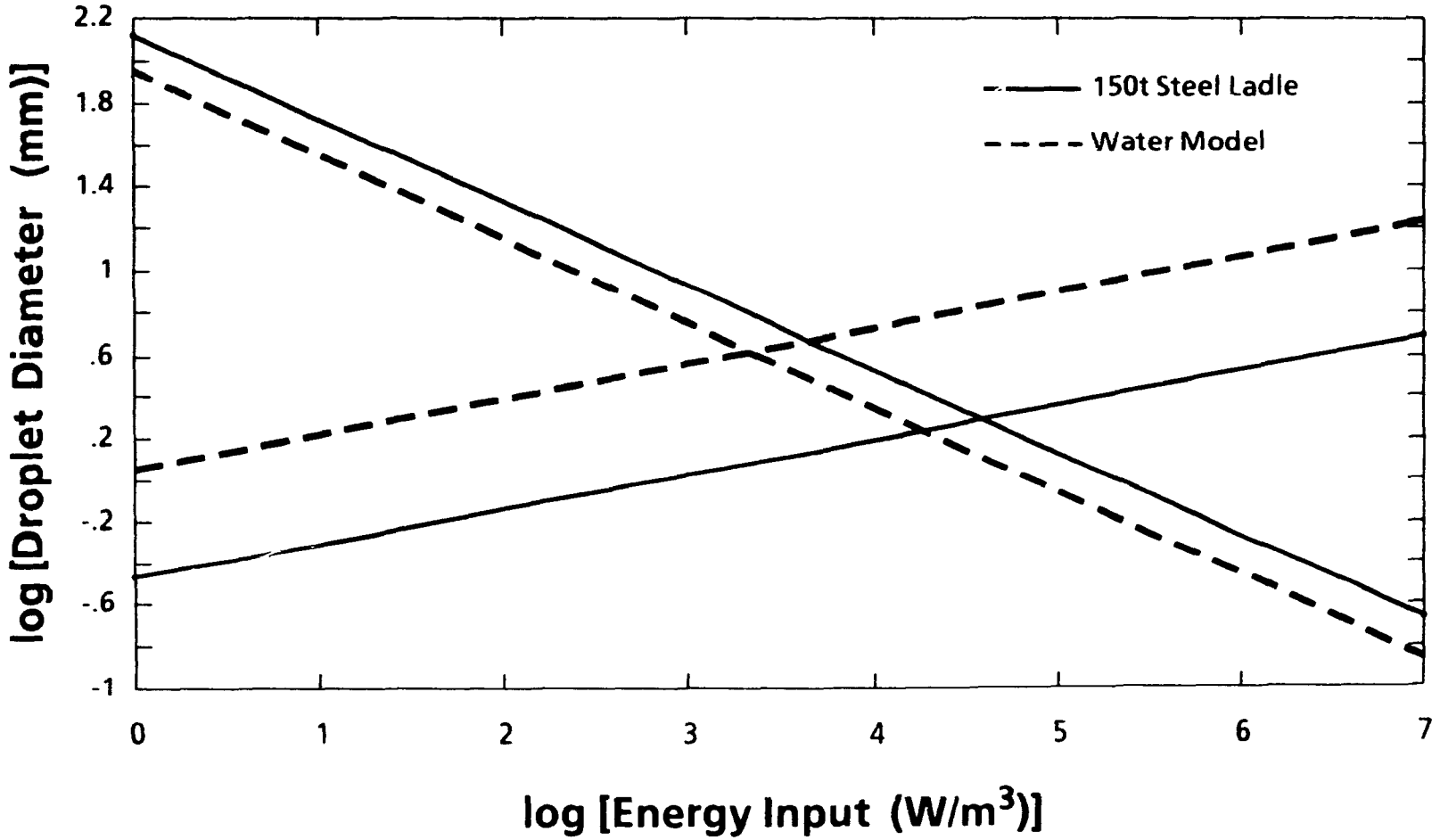

Figure 3.19 Comparison of the Size of Stable Droplets Generated and the Size of Entrained Droplets for Steel Ladle

4 CONCLUSIONS

Physical modelling of upright cylindrical vessels containing two immiscible liquids was perfromed A modified Froude number modelling criterion was used to select the operating parameters for the experiments The liquids were agitated by a single centrally located tuyere in the flat bottom of the model A range of agitation levels was employed. The goal was to determine the influence of a second liquid phase on the mixing and entrainment behaviour in gently and intensively stirred reaction vessels

The results of the experiments indicated that for a vertical cylindrical vessel filled to a height of 0.10m and with an aspect ratio of 0.33 that:

i) for low levels of energy input, the thickness and viscosity of the upper phase influences the mixing behaviour. Thicker slags increase the mixing time by altering the fluid motion in the lower phase. For thin layers, the a single recirculating flow pattern is establised, while multiple circulating zones are generated as the thickness of the layer is increased. Less viscous layers were seen to also increase the mixing time.

ii) for intensively stirred vessels, the thickness and viscosity of the upper liquid did not significantly alter the mixing behaviour Sufficient energy was supplied by the injected gas to break up the upper layer, thereby reducing the effects on fluid motion seen at the lower energy levels.

iii) a transition in the mixing behaviour occurs between the gentle and intensive systems. For lower flowrates the mixing time varied with the flowrate to the power -0.2 to -0.3. At higher flowrates the exponent changed to -0.75 to -1.0. The transition occured at a modified Froude number of approximately 3 to 4.

iv) at low energy inputs, the degree of entrainment of the upper layer is constant for a given flowrate, and increases with increasing flowrate and thickness of the layer

v) the distribution of entrained droplets at low flowrates mirrors the fluid motion: for thin layers, the droplets are distributed throughout the bath, while for thicker layers, where a tight flow loop is generated near the plume, the majority of particles are trapped near the plume.

vi) as the flowrate increases past a critical point, the number density of the entrained droplets increases rapidly The transition flowrate was found to increase with increasing thickness of the upper layer.

vii) the presence of a less dense second liquid retards the generation of a swirling motion by the plume. The precession of the plume seen the model, when no upper phase was present, could be described as forming a conical shape with the tuyere at the bottom of the model located at the apex.

During the development of the experiments used in this study it was found that dye injection and photoelectric sensing could be used to monitor the mixing behaviour of a model system The time for mixing is considerably shorter than the commonly used electrical conductivity technique since a global, rather than local, mixing behaviour is being monitored.

A system using refractive indicies and electronic circuitry was developed to effectively monitor the entrainment behaviour of one liquid into another. The system was also used successfully to differentiate between the entrainment of liquid droplets and air bubbles. The circuitry allowed for the size of the entrained droplets to be estimated.

References

1 J.R. Stubbles, The Original Steelmakers, Iron and Steel Society Inc., Warrendale, PA, 1984

2 T. Kato, Trans. ISIJ, vol. 26, 1986, pp. 851-857

3 K.S. Goto and K Nagata, Trans ISIJ, vol. 21, 1981, pp. 446-453

4 J.J. Moore, J. of Metals, vol. 34, no. 6, 1982, pp. 39-48

5 P.J. Mackey and P. Tarasoff, J. of Metals, vol. 36, no.9, 1984, pp. 21-27

6 T.R.A. Davey, Lead-Zinc-Tin '80, TMS-AIME World Symp. on Metallurgy and Environmental Control, Feb. 24-28, 1980, pp. 48-65

7 F.D. Richardson, Trans Instn. Min. & Metall., vol. 84, 1975, pp. 32-37

8 B. Berg, G. Carlsson and M. Brämming, Scand. J. of Metall., vol. 14, 1985, pp. 299-305

9 R. Siemssen and K.W. Lange, Steel Research, vol. 59, 1988, pp. 96-103

10 D Mazumdar and R.I.L. Guthrie, Met. Trans., vol. 17B, 1986, pp 725-733

11 J. Szekely and N. El Kaddah, Iron and Steelmaker, vol. 11, no. 1, 1984, pp. 22-29

12 A.H. Castillejos and J.K. Brimacombe, Met. Trans , vol. 18B, 1987, pp. 659-671

13 Y. Sahai and R I.L. Guthrie, Met. Trans., vol. 13B, 1982, pp. 193-202

14 N.A. Hussain and R. Siegel, J. of Fluids Eng., vol. 98, March 1986, pp. 49-57

15 M. Sano and K. Mori, Trans. ISIJ, vol. 23, 1983, pp 169-175

16 S. Ramani and A K. Lahiri, Steel Research, vol. 59, 1988, pp. 93-95

17 J. Szekely, T. Lehner and C.W. Wang, Ironmaking and Steelmaking, vol. 6, no. 6, 1979, pp. 285-293

18 K. Nakanishi, T. Fujii and J. Szekely, Ironmaking and Steelmaking, vol. 2, no. 3, 1975, pp. 193-197

19 O. Haida, T. Emi, S. Yamada and F Sudo, Scaninject III, paper #20

20 L.H. Lehrer, IEC Progress Design and Development, vol. 7, no 2, 1968, pp. 226-239

21 L.W. Helle, J. South Afr. Inst. of Mining and Metall., vol. 81, 1981, pp. 329-337

22. I F. Masterson, Proc. 6th Process Technology Conf., Washington, 1986, pp 377-383

23 S. Asai, T. Okamoto, J. He and I. Muchi, Trans. ISIJ, vol. 23, 1983, pp. 43-50

24 T. Stapurewicz and N.J. Themelis, Can. Met. Quarterly, vol. 26, 1987, pp. 123-128

25 U.P. Sinha and M J. McNallan, Met. Trans., vol. 16B, 1985, pp. 850-853

26 S. Paul and D.N. Ghosh, Met. Trans., vol. 17B, 1986, pp. 461-469

27 W. Shanghuai and X. Chengzhi, Iron and Steel (China), vol 21, no 10, 1986, pp.

28 S. Kim and R.J. Fruehan, Met. Trans , vol. 18B, 1987, pp. 381-390

29 D. Mazumdar, H. Nakajima and R.I.L. Guthrie, Met. Trans., vol. 19B, 1988, pp. 507-511

30 R. Matway, H. Henein, R.J. Fruehan and J. Isaacs, 4th Process Technology Conf., Chicago, 1984, pp. 39-43

31 S. Tanaka and R.I.L. Guthrie, 6th Process Technology Conf , Washington, 1986, pp. 249-255

32 H. Schlarb and M.G. Frohberg, Steel Research, vol. 56, 1985, pp. 15-18

33 S. Tanaka, "Modelling Inclusion Behaviour and Slag Entrainment in Liquid Steel Processing Vessels", PhD thesis, McGill University, 1986.

34 R. Guthrie, Engineering in Process Metallurgy, Oxford University Press , 1988

35 B. Külünk, M.Eng. thesis, McGill University, Montreal, 1987

36 D. Mazumdar and R.I.L. Guthrie, Met. Trans., vol. 16B, 1985, pp. 83-90

37 P.V. Riboud and L.D Lucas, Can. Met. Quarterly, vol. 20, 1981, pp. 199-208

38 S. Kim, PhD. thesis, Carnagie-Mellon University, Pittsburgh, 1986

39 H Gaye, L.D. Lucas, M. Olette and P.V. Riboud, Can. Met. Quarterly, vol. 23, 1984, pp. 179-191

40 A. Mersmann, A Short Course on Mixing Technology, Dept. of Chemical Eng., McGill University, Montreal, July 26-28, 1982, pp. 6/1-6/6.

41 J. Mietz and F. Oeters, Steel Research, vol. 59, 1988, pp. 52-59

42 S. Joo and R.I.L. Guthrie, Int. Symp. on Ladle Steelmaking and Furnaces, 27th Annual Conference of Metallurgists, Montreal, 1988, pp.1-28

43 D.S. Conochie and N.B. Gray, Trans. Instn. Min. & Metall., vol. 81, March 1979, pp. C14-C18

44 C.K. Coyle, AIChE Journal, vol. 16, 1970, pp. 903-906

45 Y. Mlynek and W Resnick, AIChE Journal, vol. 18, 1972, pp. 122-127

46 G. Narsimhan, D. Ramkrishna and J.P. Gupta, AIChE Journal, vol. 26, 1980, pp. 991-1000

47 H. Nakajima, Ph.D. thesis, McGill University, Montreal, 1987.

48 G.G. Krishna Murthy, S.P. Mahrotra and A. Ghosh, Met. Trans , vol 19B, Dec. 1988, pp. 839-850.

49 Y. Kato, T. Nozaki, K. Nakanishi, T. Fujii, and T. Emi, Tetsu-to-Hagane, vol 70, pp.380-387, (Translation by Mr. M Yoshioka for BHP Central Research Laboratories, Nov. 1985)

50 Roy J. Matway, "Physical Modeling of Liquid/Liquid Mass Transfer with Submerged Gas Injection", PhD thesis, Carnegie-Mellon University, 1986.

51 Y. Sahai, R.I.L. Guthrie, Met. Trans., vol 13B, 1982, pp. 203-211.

52 G.G. Krishna Murthy, S.P. Mehrotra and A. Ghosh, 6th Process Technology Conference, Washington, 1986, pp. 401-407.

53 O. Haida and J.K. Brimacombe, Scaninject III, paper # 5.

54 L. Liu, T. Kaiwen, and D. Ting, Proceedings Technological Advances in Metallurgy, Lulea, Sweden Sept. 20-21, 1988, Paper #6.

APPENDIX

CALCULATIONS OF DROPLET SIZE BASED UPON SENSOR REPSONSE TIME

Example 1. Droplet diameter is less than or equal to the internal diameter of the collection tube.

In this case, the droplet remains spherical in the tube and the length of the droplet, as measured by the sensor, will be equal to its diameter.

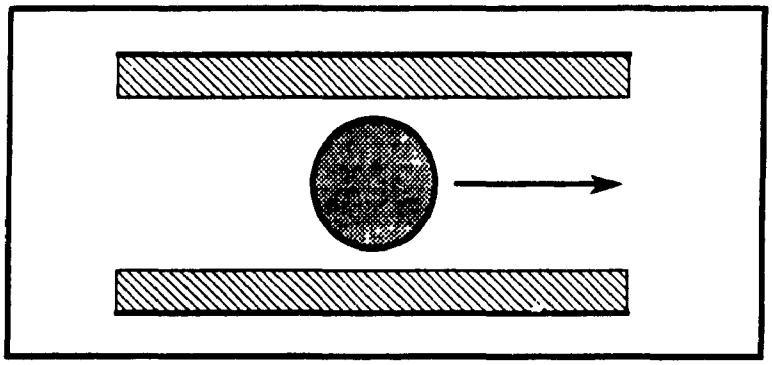

Assumptions:

Internal Diameter of Tube = 1.19mm
Fluid Extraction Rate = 40 ml/min
Sensor response time = 1 msec

$$\textbf{Mean Fluid Velocity} = \frac{\text{Fluid Extraction Rate}}{\text{Tube Cross sectional Area}}$$

$$= \left(\frac{40\ \text{cm}^3}{60\ \text{sec}}\right)\left(\frac{4}{\pi\ (0.119\text{cm})^2}\right) = 599.4\ \text{mm/sec}$$

$$\textbf{Droplet Diameter} = (\text{Fluid Velocity} * \text{Response Time}) = (599\ 4 * \frac{1}{1000}) = 0\ 60\text{mm}$$

Example 2. Droplet diameter is greater than the internal diameter of the collection tube.

In this case, the droplet will be elongated and have rounded ends. The diameter of the elongated section is assumed to be equal to the internal diameter of the tubing

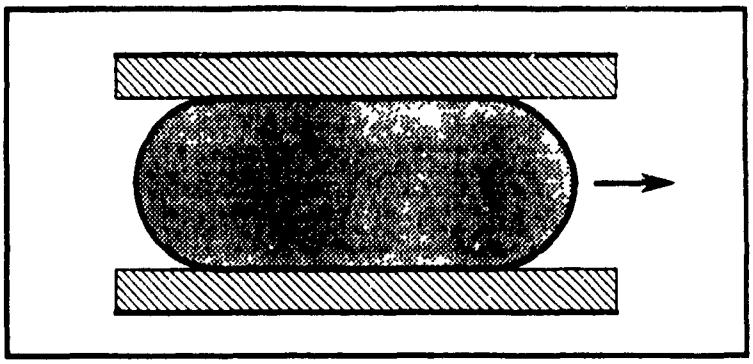

Assumptions:

Internal Diameter of Tube = 1.19mm
Fluid Extraction Rate = 40 ml/min
Sensor response time = 10 msec
Droplet is Cylindrical in Shape (i.e. ignore rounded ends)

$$\textbf{Mean Fluid Velocity} = \frac{\text{Fluid Extraction Rate}}{\text{Tube Cross sectional Area}}$$

$$= \left(\frac{40\ \text{cm}^3}{60\ \text{sec}}\right)\left(\frac{4}{\pi\ (0\ 119\text{cm})^2}\right) = 599\ 4\ \text{mm/sec}$$

$$\textbf{Droplet Length} = (\text{Fluid Velocity} * \text{Response Time}) = \left(599\ 4 * \frac{10}{1000}\right) = 5\ 99\text{mm}$$

$$\textbf{Droplet Volume} = (\text{Droplet Length} * \text{Tube Area}) = \left(5\ 99\text{mm} * \frac{\pi(1\ 19mm)^2}{4}\right) = 6\ 66\text{mm}^3$$

$$\textbf{Equivalent Droplet Diameter} = \left(\frac{6 * \text{Volume}}{\pi}\right)^{1/3} = \left(\frac{6 * 6\ 66}{\pi}\right)^{1/3} = 2\ 33\text{mm}$$

The following graphs shows the droplet diameters calculated for a range of response times at two different fluid extraction rates, namely 40 and 60 ml/min.